VNHC and Acrobot Title

Adan Moran-MacDonald, *Member, IEEE*, Manfredi Maggiore, *Member, IEEE**, and Xingbo Wang

Abstract

In this article we study virtual nonholonomic constraints, which are relations between the generalized coordinates and generalized momenta of a mechanical system that can be enforced via feedback control. We design a constraint which emulates gymnastics giant motion in an acrobot, and rigorously prove that this constraint will inject or dissipate energy. This constraint is tested in simulation and on a real-world acrobot, demonstrating highly effective energy regulation properties and robustness to a variety of disturbances.

Index Terms

energy regulation, virtual nonholonomic constraints, acrobot, gymnastics.

I. Introduction

In gymnastics terminology, a "giant" is the motion a gymnast performs to achieve full rotations around a horizontal bar [1]. A gymnast will begin by hanging at rest, then swing their legs appropriately to gain energy over time. The authors of [2] modelled the gymnast as a variable length pendulum, and studied how the pendulum's length changes as a function of the gymnast's limb angle. Labeling the pendulum length by r and the gymnast's body orientation by θ, they observed experimentally that the value $\dot{r}/r$ has the biggest impact on the magnitude of energy injection. After testing several gymnasts under a variety of experimental conditions, they discovered that the peak value of $\dot{r}/r$ occured at the same fixed value of $\dot{\theta}/\theta$ for all gymnasts. In other words, gymnasts appear to move their legs as a function of their body angle and velocity when performing giants; doing so allows them to gain energy and rotate around the bar.

While the simplest model of a gymnast is the variable-length pendulum, a more realistic model is the two-link acrobot (Figure 1). Here, the top link represents the torso while the bottom link represents the legs. The acrobot is actuated exclusively at the center joint (the hips). Controlling the acrobot is a nontrivial task because it is not feedback linearizable [3]. To solve the swingup problem, one might begin by designing a leg controller which provably injects energy into the acrobot, so that the resulting motion mimics that of a human performing a giant.

Previous attempts at acrobot giant generation have involved trajectory tracking, partial feedback linearization, or other energy-based methods (see [5]–[8]). While all these approaches succeed at making the acrobot rotate around the bar, none of them use the results of [2]. That is, none of these leg controllers track a function of the acrobot's body angle and velocity. In 2016, Wang designed a controller [4] which tracked the body angle and an *estimate* of the velocity, but not the velocity itself. His approach was a preliminary version of a recent technique know as the method of virtual nonholonomic constraints [9].

Manuscript submitted for review on June 7, 2021.

A. Moran-MacDonald (e-mail: adan.moran@mail.utoronto.ca) and M. Maggiore (e-mail: maggiore@control.utoronto.ca) are with the Department of Electrical and Computer Engineering, University of Toronto, ON, Canada.

X. Wang is with ??? (e-mail: ???).

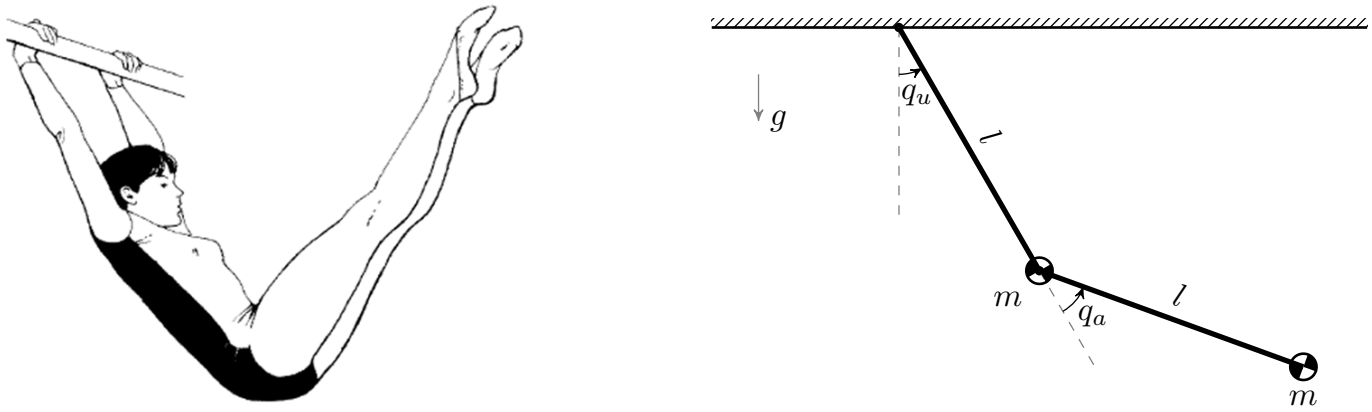

Fig. 1: A simplified two-link acrobot as a model for a gymnast. Image modified from [4].

Virtual nonholonomic constraints (VNHCs) have been used for human-robot interaction [10]–[12], error-reduction on time-delayed systems [13], and they have shown marked improvements to the field of bipedal locomotion [9], [14], [15]. Indeed, they produce more robust walking motion in biped robots than other virtual constraints which do not depend on velocity [16]. In particular, VNHCs may be capable of injecting and dissipating energy from a system in a robust manner, all while producing realistic biological motion.

In this article, we will design a virtual nonholonomic constraint which provably injects energy into the acrobot through human-like giant motion. In particular, any acrobot constrained by this VNHC is guaranteed to perform rotations around the bar. Under suitable conditions on the acrobot's physical parameters, this VNHC also enables the acrobot to rotate around the bar at a desired speed. We will provide simulations to show how one can use VNHCs to regulate energy, along with experimental results which demonstrate the robustness of this behaviour to model uncertainty, sensor noise, and a variety of external disturbances.

Notation: We use the following notation and terminology in this article. The $n \times n$ identity matrix is denoted I_n, and the $n \times m$ matrix of zeros is denoted $\mathbf{0}_{n\times m}$. A matrix $A \in \mathbb{R}^{n\times m}$ is *right semi-orthogonal* if $AA^\mathsf{T} = I_n$ and is *left semi-orthogonal* if $A^\mathsf{T}A = I_m$. For $A \in \mathbb{R}^{n\times m}$ and $B \in \mathbb{R}^{p\times m}$, we define $[A; B] \in \mathbb{R}^{(n+p)\times m}$ as the matrix obtained by stacking A on top of B. Given $\sigma_1, \ldots, \sigma_n \in \mathbb{R}$, we define $\operatorname{diag}(\sigma_1, \ldots, \sigma_n) \in \mathbb{R}^{n\times n}$ as the diagonal matrix whose value at row i, column i is σ_i. For $T > 0$, the set of real numbers modulo T is denoted $[\mathbb{R}]_T$, with $[\mathbb{R}]_\infty := \mathbb{R}$. The gradient of a matrix-valued function $A : \mathbb{R}^m \to \mathbb{R}^{n\times n}$ is the block matrix of stacked partial derivatives, $\nabla_x A := [\partial A/\partial x_1; \cdots; \partial A/\partial x_m] \in \mathbb{R}^{nm\times n}$. Given two matrices $A \in \mathbb{R}^{n\times m}$ and $B \in \mathbb{R}^{r\times s}$, the Kronecker product (see [17]) is the matrix $A \otimes B \in \mathbb{R}^{nr\times ms}$ defined as

$$A \otimes B = \begin{bmatrix} A_{1,1}B & \cdots & A_{1,m}B \\ \vdots & \ddots & \vdots \\ A_{n,1}B & \cdots & A_{n,m}B \end{bmatrix}. \tag{1}$$

The Poisson bracket [18] between the functions $f(q,p)$ and $g(q,p)$ is

$$[f,g] := \sum_{i=1}^{n} \frac{\partial f}{\partial p_i}\frac{\partial g}{\partial q_i} - \frac{\partial f}{\partial q_i}\frac{\partial g}{\partial p_i}. \tag{2}$$

The Kronecker delta δ_i^j is 1 if $i = j$ and 0 otherwise. Finally, we say a function $R(I)$ is $O(I^2)$ if $\lim_{I\to 0} R(I)/I = 0$.

II. Problem Formulation

We will use the simplified acrobot model in Figure 1, where we assume the torso and leg rods are of equal length l with equal point masses m at the tips. The acrobot's configuration is described in generalized coordinates (q_u, q_a) on the configuration manifold $\mathcal{Q} = \mathbb{S}^1 \times \mathbb{S}^1$, where q_u is unactuated and q_a is actuated. A real gymnast cannot swing their legs in full circles, though they are usually flexible enough to raise them parallel to the floor; hence, we assume the leg angle q_a lies in $[-Q_a, Q_a]$ for some $Q_a \in [\frac{\pi}{2}, \pi[$. We also ignore any dissipative forces.

The acrobot has inertia matrix M, potential function V (with respect to the horizontal bar), and input matrix B given as follows:

$$M(q) = \begin{bmatrix} ml^2(3 + 2\cos(q_a)) & ml^2(1 + \cos(q_a)) \\ ml^2(1 + \cos(q_a)) & ml^2 \end{bmatrix}, \tag{3}$$

$$V(q) = -mgl(2\cos(q_u) + \cos(q_u + q_a)), \tag{4}$$

$$B = [0; 1]. \tag{5}$$

For reasons that will become clear in later sections of this article, we will use Hamiltonian mechanics to derive the dynamics of the acrobot. For this we require the conjugate of momenta, $p = (p_u, p_a) = M(q)\dot{q}$. The dynamics of the acrobot in (q,p) coordinates are given in (6). For shorthand, we write $c_u := \cos(q_u)$, $c_a := \cos(q_a)$, and $c_{ua} := \cos(q_u + q_a)$; likewise, $s_u := \sin(q_u)$, $s_a := \sin(q_a)$, and $s_{ua} := \sin(q_u + q_a)$.

$$\mathcal{H}(q,p) = \frac{1}{2}p^\mathsf{T}M^{-1}(q)p - mgl(2c_u + c_{ua}), \tag{6}$$

$$\begin{cases} \dot{q} = M^{-1}(q)p, \\ \dot{p}_u = -mgl(2s_u + s_{ua}), \\ \dot{p}_a = -\frac{1}{2}p^\mathsf{T}\nabla_{q_a}M^{-1}(q)p - mgls_{ua} + \tau. \end{cases}$$

The control input is a force $\tau \in \mathbb{R}$ affecting only the dynamics of p_a, representing a torque acting on the hip joint. Let us now define what it means for a mechanical system to gain or lose energy.

Definition 1: Let $\mathcal{Q}$ be an n-dimensional smooth manifold. Let $f : \mathcal{Q} \to T\mathcal{Q}$ be a smooth vector field and let $D \subset \mathcal{Q}$ be open. The system described by $\dot{x} = f(x)$ *gains energy on* D if, for all compact sets $K \subset D$ and for almost every initial

condition $x(0) \in K$, there exists $T > 0$ such that $x(t) \notin K$ for all $t > T$. The system *loses energy on* D if it gains energy in negative-time.

Our goal is to design a smooth function $f : \mathbb{S}^1 \times \mathbb{R}$ such that the relation $q_a = f(q_u, p_u)$ for system (6) can be enforced asymptotically via feedback control (in Section III we call this a regular virtual nonholonomic constraint). We will further require that the dynamics of the acrobot, when the relation holds, gain or lose energy on some set D in the sense of Definition 1.

Note that any system satisfying Definition 1 can have unstable equilibria on D, but not limit cycles nor closed orbits.

III. Theory of VNHCs

Before embarking on our design problem, we must summarize the relevant theory of virtual nonholonomic constraints for a class of mechanical systems we call "simply actuated hamiltonian systems". Note that the results we provide in Section III-B are not novel: they are a special case of the results in [9].

A. Simply Actuated Hamiltonian Systems

Take a mechanical system modelled with generalized coordinates $q = (q_1, \dots, q_n)$ on a configuration manifold $\mathcal{Q} = [\mathbb{R}]_{T_1} \times \cdots \times [\mathbb{R}]_{T_n}$, where $T_i = 2\pi$ if q_i is an angle and $T_i = \infty$ if q_i is a displacement. The corresponding generalized velocities are $\dot{q} = (\dot{q}_1, \dots, \dot{q}_n) \in \mathbb{R}^n$.

Suppose this system has Lagrangian $\mathcal{L}(q, \dot{q}) = 1/2\ \dot{q}^T D(q)\dot{q} - P(q)$, where the potential energy $P : \mathcal{Q} \to \mathbb{R}$ is smooth, and the inertia matrix $D : \mathcal{Q} \to \mathbb{R}^{n\times n}$ is smooth and positive definite for all $q \in \mathcal{Q}$. The *conjugate of momentum* to q is the vector $p := \partial\mathcal{L}/\partial\dot{q} = D(q)\dot{q} \in \mathbb{R}^n$. As per [18], the *Hamiltonian* of the system in (q, p) coordinates is

$$\mathcal{H}(q, p) = \frac{1}{2} p^{\mathsf{T}} D^{-1}(q) p + P(q), \tag{7}$$

with dynamics

$$\begin{cases} \dot{q} = \nabla_p \mathcal{H}, \\ \dot{p} = -\nabla_q \mathcal{H} + B(q)\tau, \end{cases} \tag{8}$$

where $\tau \in \mathbb{R}^k$ is a vector of generalized input forces and the input matrix $B : \mathcal{Q} \to \mathbb{R}^{n\times k}$ is full rank for all $q \in \mathcal{Q}$. If $k < n$, we say the system is *underactuated* with degree of underactuation $(n - k)$.

Using the matrix Kronecker product, it is easy to show that (8) expands to

$$\begin{cases} \dot{q} = D^{-1}(q)p, \\ \dot{p} = -\frac{1}{2}(I_n \otimes p^{\mathsf{T}})\nabla_q D^{-1}(q)p - \nabla_q P(q) + B(q)\tau. \end{cases}$$

Because τ is transformed by $B(q)$, it is not obvious how any particular input force τ_i affects the system. As a first step in addressing this problem, we make the following assumptions.

Assumption 1: The input matrix $B(q) \equiv B \in \mathbb{R}^{n\times k}$ is constant, full rank, and $k < n$.

Assumption 2: There exists a right semi-orthogonal matrix $B^\perp \in \mathbb{R}^{(n-k)\times n}$ which is a left-annihilator for B.

Note that Assumption 2 requires the rows of $B^\perp$ be unit vectors that are mutually orthogonal. When $k = (n-1)$, Assumption 2 can be removed because it is automatically implied by Assumption 1.

The above assumptions allow us to define a canonical coordinate transformation of (7) which decouples the input forces. To define this transformation we will make use of the following lemma.

Lemma 1: Suppose Assumption 1 holds. Then there exists a nonsingular matrix $\hat{T} \in \mathbb{R}^{k\times k}$ so that the regular feedback transformation

$$\tau = \hat{T}\hat{\tau}$$

has a new input matrix $\hat{B}$ for $\hat{\tau}$ which is left semi-orthogonal.

Proof: Since B is constant and full rank, it has a singular value decomposition $B = U^{\mathsf{T}}\Sigma V$ where $\Sigma = [\mathrm{diag}\,(\sigma_1, \dots, \sigma_k)\,; \mathbf{0}_{(n-k)\times k}]$, $\sigma_i > 0$, and $U \in R^{n\times n}$, $V \in \mathbb{R}^{k\times k}$ are unitary matrices [19]. Defining $T = \mathrm{diag}\,(1/\sigma_1, \dots, 1/\sigma_k)$ and assigning the regular feedback transformation $\tau = VT\hat{\tau}$ yields a new input matrix $\hat{B} = BVT$ for $\hat{\tau}$ such that $\hat{B}^{\mathsf{T}}\hat{B} = T^{\mathsf{T}}\Sigma^{\mathsf{T}}\Sigma T = I_k$. ∎

In light of Lemma 1 there is no loss of generality in assuming that the input matrix is left semi-orthogonal, which means that B^{T} is right semi-orthogonal. Now, let $\mathbf{B} := [B^\perp; B^{\mathsf{T}}]$. Since $B^\perp$ is a left annihilator of B and both $B^\perp$ and B^{T} are right semi-orthogonal, one can easily show that $\mathbf{B}$ is an orthogonal matrix.

We temporarily take $\mathcal{Q}$ to be embedded in $\mathbb{R}^N$ so that the transformation $\tilde{q} = \mathbf{B}q$ is well-defined.

Theorem 1: Take the Hamiltonian system (7) and suppose Assumptions 1 and 2 hold. The coordinate transformation $(\tilde{q} = \mathbf{B}q, \tilde{p} = \mathbf{B}p)$ is a canonical transformation and the resulting dynamics are given by

$$\mathcal{H}(\tilde{q},\tilde{p}) = \frac{1}{2}\tilde{p}^{\mathsf{T}} M^{-1}(\tilde{q})\tilde{p} + V(\tilde{q}), \tag{9}$$

$$\begin{cases} \dot{\tilde{q}} = M^{-1}(\tilde{q})\tilde{p}, \\ \dot{\tilde{p}} = -\frac{1}{2}(I_n \otimes \tilde{p}^{\mathsf{T}})\nabla_{\tilde{q}} M^{-1}(\tilde{q})\tilde{p} \\ \qquad\quad - \nabla_{\tilde{q}} V(\tilde{q}) + \begin{bmatrix} \mathbf{0}_{(n-k)\times k} \\ I_k \end{bmatrix} \tau, \end{cases}$$

where $M^{-1}(\tilde{q}) := \mathbf{B}D^{-1}(\mathbf{B}^{\mathsf{T}}\tilde{q})\mathbf{B}^{\mathsf{T}}$ and $V(\tilde{q}) := P(\mathbf{B}^{\mathsf{T}}\tilde{q})$.

Proof: Since $\mathbf{B}$ is constant, this transformation satisfies $\partial\tilde{q}_i/\partial p_j = \partial\tilde{p}_i/\partial q_j = 0$ for all $i, j \in \{1,\dots,n\}$. This implies the Poisson brackets $[\tilde{q}_i, \tilde{q}_j]$ and $[\tilde{p}_i, \tilde{p}_j]$ are both zero. Then, since $\mathbf{B}$ is orthogonal, $[\tilde{p}_i, \tilde{q}_j] = (\mathbf{B}_i)^{\mathsf{T}}(\mathbf{B}^{\mathsf{T}})_j = \delta_i^j$. By (45.10) in [18], this is a canonical transformation and the new Hamiltonian is $\mathcal{H}(\mathbf{B}^{\mathsf{T}}\tilde{q}, \mathbf{B}^{\mathsf{T}}\tilde{p})$. Finally, since $\dot{\tilde{p}} = \mathbf{B}\dot{p}$, the input matrix for the system in $(\tilde{q},\tilde{p})$ coordinates is $\mathbf{B}B = [\mathbf{0}_{(n-k)\times k}; I_k]$, which proves the theorem. ■

We call the $(\tilde{q},\tilde{p})$ coordinates *simply actuated coordinates*, and we call system (9) a *simply actuated hamiltonian system*. The first $(n-k)$ configuration variables in $\tilde{q}$, labelled q_u, are the *unactuated coordinates*; the remaining k configuration variables, labelled q_a, are the *actuated coordinates*. The corresponding (p_u, p_a) in $\tilde{p}$ are the *unactuated* and *actuated momenta*, respectively.

B. Virtual Nonholonomic Constraints

Griffin and Grizzle [14] were the first to define relative degree two nonholonomic constraints which can be enforced through state feedback. Horn *et al.* later extended their results in [9] to derive the constrained dynamics for a certain class of mechanical systems. These researchers made use of the unactuated conjugate of momentum, but they developed their results in the Lagrangian framework. In particular, they focused on Lagrangian systems with degree of underactuation one. We will now present a special case of [9] for simply actuated hamiltonian systems, so that the theory we apply to the acrobot is provided in its clearest form. After we finish this summary we will clarify the relationship between our material and that of [9].

For the rest of this section we take the system of inquiry to be a Hamiltonian mechanical system in simply actuated coordinates, as in (9). For simplicity of notation, we relabel $(\tilde{q},\tilde{p})$ to (q,p).

Definition 2: A *virtual nonholonomic constraint* (VNHC) *of order* k is a relation $h(q,p) = 0$ where $h : \mathcal{Q} \times \mathbb{R}^n \to \mathbb{R}^k$ is C^2, $\operatorname{rank}([dh_q,\, dh_p]) = k$ for all $(q,p) \in h^{-1}(0)$, and there exists a feedback controller $\tau(q,p)$ rendering the *constraint manifold* Γ invariant, where

$$\Gamma = \{(q,p) \mid h(q,p) = 0, dh_q\dot{q} + dh_p\dot{p} = 0\}. \tag{10}$$

The constraint manifold is a $2(n-k)$-dimensional closed embedded submanifold of $\mathcal{Q}\times\mathbb{R}^n$. A VNHC thereby allows us to study a reduced-order model of the system: it reduces the original $2n$ differential equations to $2(n-k)$ equations. In particular, if $k = (n-1)$, the constraint manifold is *always* 2-dimensional and its dynamics can be plotted on a plane.

In order to enforce the constraint $h(q,p) = 0$, we want to asymptotically stabilize the set Γ. To see when this is possible, let us define the error output $e = h(q,p)$. If any component of e_i has relative degree 1, we may not be able to stabilize Γ: we can always guarantee $e_i \to 0$, but not necessarily $\dot{e}_i \to 0$. It is for this reason that we define the following special type of VNHC.

Definition 3: A VNHC $h(q,p) = 0$ of order k is *regular* if the output $e = h(q,p)$ is of relative degree $\{2, 2\dots, 2\}$ everywhere on the constraint manifold Γ.

The authors of [9], [14] observed that relations which use only the unactuated conjugate of momentum often have vector relative degree $\{2,\dots,2\}$. Indeed, we shall now provide a characterization of regularity which shows that regular constraints cannot use the actuated momentum at all.

To ease notation in the rest of this section, we use the following shorthand:

$$\mathcal{A}(q,p_u) := dh_q(q,p_u)M^{-1}(q), \tag{11}$$

$$\mathcal{M}(q,p) := (I_{n-k} \otimes p^{\mathsf{T}})\nabla_{q_u} M^{-1}(q). \tag{12}$$

Theorem 2: A relation $h(q,p) = 0$ for system (9) is a regular VNHC of order k if and only if $dh_{p_a} = \mathbf{0}_{k\times k}$ and the decoupling matrix

$$(\mathcal{A}(q,p_u) - dh_{p_u}\mathcal{M}(q,p)) \begin{bmatrix} \mathbf{0}_{(n-k)\times k} \\ I_k \end{bmatrix}, \tag{13}$$

is full rank k everywhere on the constraint manifold Γ.

Proof: Let $e = h(q,p) \in \mathbb{R}^k$. If $dh_{p_a} \neq \mathbf{0}_{k\times k}$ for some $(q,p) \in \Gamma$, then τ appears in $\dot{e}$ and the VNHC is not of relative degree $\{2,\dots,2\}$. Suppose now that $dh_{p_a} = \mathbf{0}_{k\times k}$. Then $\dot{e} = \mathcal{A}(q,p_u)p - dh_{p_u}\left(1/2\ \mathcal{M}(q,p)p + \nabla_{q_u}V(q)\right)$. Taking

one further derivative provides $\ddot{e} = (\star) - dh_{p_u}\left(1/2\ d/dt\left(\mathcal{M}(q,p)p\right)\right) + \mathcal{A}(q,p_u)[\mathbf{0}_{(n-k)\times k}; I_k]\tau$, where $(\star)$ is a continuous function of q and p. One can further show that $dh_{p_u}\left(1/2\ d/dt\ \ (\mathcal{M}(q,p)p)\right) = (\star) + dh_{p_u}\mathcal{M}(q,p)[\mathbf{0}_{(n-k)\times k}; I_k]\tau$. Hence,

$$\ddot{e} = (\star) + \left(\mathcal{A}(q,p_u) - dh_{p_u}\mathcal{M}(q,p)\right)\begin{bmatrix}\mathbf{0}_{(n-k)\times k}\\ I_k\end{bmatrix}\tau,$$

which we write as $\ddot{e} = E(q,p) + H(q,p)\tau$ for appropriate E and H. From the definition of regularity, the VNHC h is regular when e is of relative degree $\{2,\dots,2\}$, which is true if and only if the matrix premultiplying τ is nonsingular, and hence that H is invertible. This proves the theorem. ∎

Under additional mild conditions (see [20]), a regular VNHC of order k can be stabilized by the output-linearizing state-feedback controller

$$\tau(q,p) = -H^{-1}(q,p)\left(E(q,p) + k_p e + k_d \dot{e}\right), \tag{14}$$

where $k_p, k_d > 0$ are control parameters which can be tuned on the resulting error dynamices $\ddot{e} = -k_p e - k_d \dot{e}$.

In Section IV we will enforce a regular constraint on the acrobot of the form $h(q,p) = q_a - f(q_u,p_u)$, where the actuators track a function of the unactuated variables. Regular constraints of this form always meet the mild conditions from [20], and hence we can stabilize the constraint manifold using (14). Since q_a is constrained to be a function of the unactuated variables, intuition tells us the constrained dynamics should be parameterized by (q_u,p_u). Unfortunately, $\dot{q}_u$ depends on p_a, and for general systems one cannot solve explicitly for p_a in terms of (q_u,p_u) because the $\dot{p}$ dynamics contain the coupling term $(I_n \otimes p^{\mathsf{T}})\nabla_q M(q)p$. We now introduce an assumption which allows us to solve for p_a as a function of (q_u,p_u), which in turn allows us to explicitly solve for the constrained dynamics.

Assumption 3: The inertia matrix does not depend on the unactuated coordinates, i.e., $\nabla_{q_u} M(q) = \mathbf{0}_{n(n-k)\times n}$.

Theorem 3: Let $\mathcal{H}$ be a hamiltonian system in simply actuated form (9) satisfying Assumption 3. Let $h(q,p_u) = q_a - f(q_u,p_u)$ be a regular VNHC of order k with constraint manifold Γ. Then the constrained dynamics are given by

$$\left.\begin{aligned}\dot{q}_u &= \begin{bmatrix}I_{(n-k)} & \mathbf{0}_{(n-k)\times k}\end{bmatrix} M^{-1}(q)p\\ \dot{p}_u &= -\nabla_{q_u} V(q)\end{aligned}\right|\begin{aligned}q_a &= f(q_u,p_u)\\ p_a &= g(q_u,p_u)\end{aligned}, \tag{15}$$

where

$$g(q_u,p_u) := \left(\mathcal{A}(q,p_u)\begin{bmatrix}\mathbf{0}_{(n-k)\times k}\\ I_k\end{bmatrix}\right)^{-1}\cdot\Big(dh_{p_u}\nabla_{q_u}V(q) - \mathcal{A}(q,p_u)\begin{bmatrix}I_{(n-k)}\\ \mathbf{0}_{k\times(n-k)}\end{bmatrix}p_u\Big)\Big|_{q_a = f(q_u,p_u)}. \tag{16}$$

Proof: Setting $e = h(q,p_u)$ and using Assumption 3, we find that $\dot{e} = \mathcal{A}(q,p_u)p - dh_{p_u}\nabla_{q_u}V(q)$. Notice that $\mathcal{A}(q,p_u)p = \mathcal{A}(q,p_u)[\mathbf{0}_{(n-k)\times k}; I_k]p_a + \mathcal{A}(q,p_u)[I_{n-k}; \mathbf{0}_{k\times(n-k)}]p_u$. Since $h(q,p_u)$ is regular, $\mathcal{A}(q,p_u)[\mathbf{0}_{(n-k)\times k}; I_k]$ is invertible. Taking $e = \dot{e} = 0$, solving for p_a, and setting $q_a = f(q_u,p_u)$ completes the proof. ∎

We conclude this section by formalizing the notion of energy injection/dissipation for VNHCs.

Definition 4: A regular VNHC $h(q,p_u) = q_a - f(q_u,p_u)$ with constraint manifold Γ *injects (dissipates) energy on* $D \subset \Gamma$ if the constrained dynamics gain (lose) energy everywhere on D according to Definition 1, except possibly on a set of measure zero.

Comparison with existing literature: Horn *et al.* provide the constrained dynamics for VNHCs in [16]. Their assumption **H2** is what we call regularity, and our requirement that one can solve for $q_a = f(q_u,p_u)$ on Γ implies their assumption **H3** holds true. The only real distinction between this section and their work is that our constrained dynamics are explicit functions of the Hamiltonian coordinates (q_u,p_u). In fact, one can show that the constrained dynamics (15) coincide with the constrained dynamics in [9, Eqn. (17)] when one chooses the special case $\theta_1 = q_u$ and $\theta_2 = p_u$. This explicit representation will be beneficial when we apply the theory of VNHCs to the acrobot.

IV. The Acrobot VNHC

Our goal in this article is to design a VNHC which injects energy into the acrobot by means of a giant-like motion. Recall that the acrobot in Figure 1 has dynamics given by (6), repeated here for convenience:

$$\begin{cases}\dot{q} = M^{-1}(q)p,\\ \dot{p}_u = -mgl\left(2s_u + s_{ua}\right),\\ \dot{p}_a = -\frac{1}{2}p^{\mathsf{T}}\nabla_{q_a}M^{-1}(q)p - mgls_{ua} + \tau.\end{cases}$$

Since the control input τ only affects the actuated momentum, the system above is already in simply actuated form. Its state space is $\mathcal{Q}\times\mathcal{P}$ where $\mathcal{Q} = \mathbb{S}^1\times\mathbb{S}^1$, and $\mathcal{P} = \mathbb{R}\times\mathbb{R}$. We can therefore apply the theory from Section III to design a VNHC of the form $q_a = f(q_u,p_u)$ (i.e., a VNHC $h(q,p_u) = q_a - f(q_u,p_u) = 0$). Since we need the VNHC to be regular, the following proposition will be useful.

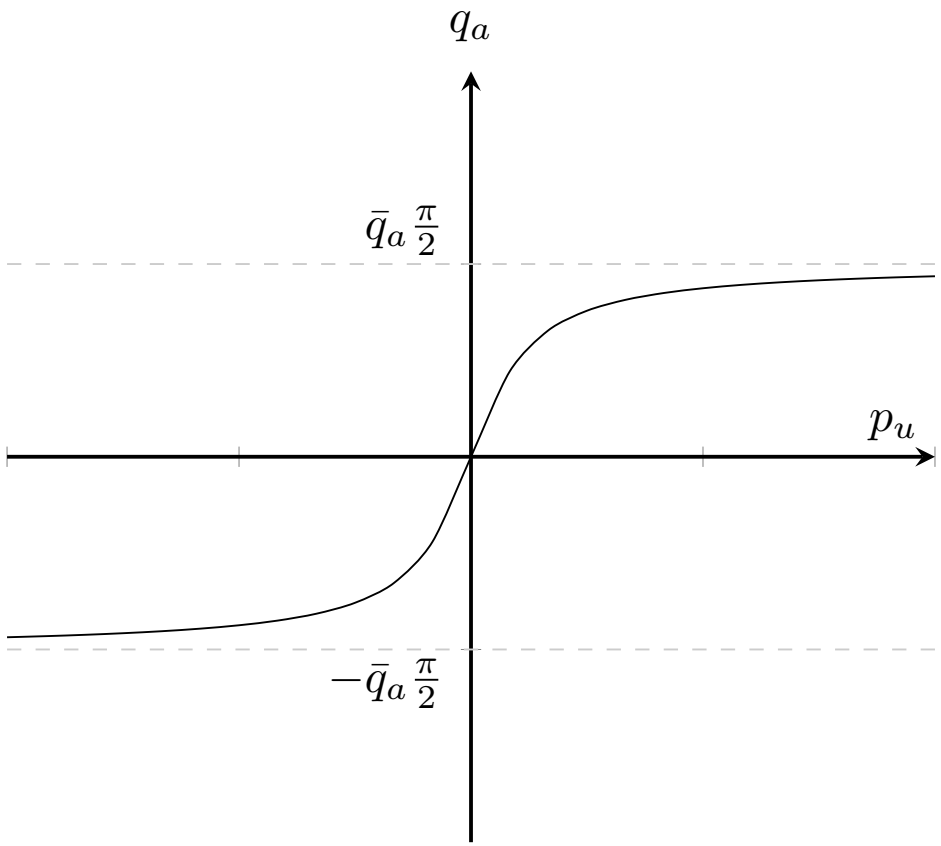

Fig. 2: The acrobot constraint $q_a = \bar{q}_a \arctan(Ip_u)$.

Proposition 1: Any relation $q_a = f(p_u)$ with $f \in C^2\left(\mathbb{R}; \mathbb{S}^1\right)$ is a regular VNHC of order 1 for the acrobot.

Proof: The decoupling matrix (13) for the acrobot evaluates to $((1+c_a)\partial_{q_u} f(q_u, p_u) + (3+2c_a))/(ml^2(2-c_a^2))$. Since $\partial_{q_u} f = 0$, this matrix is strictly positive for all values of q_a, and hence is full rank 1 everywhere on the constraint manifold. ■

To design our VNHC, we begin by examining a person on a seated swing. The person extends their legs when the swing moves forwards, and retracts their legs when the swing moves backwards. As the swing gains speed, the person leans their body while extending their legs higher, thereby shortening the distance from their center of mass to the pivot and adding more energy to the swing [21].

Now imagine the person's torso is affixed to the swing's rope so they are always upright. Imagine further that the swing has no seat at all, allowing the person to extend their legs beneath them. This position is identical to that of a gymnast on a bar.

The acrobot's legs are rigid rods which cannot retract, so we emulate the person on a swing by pivoting the legs toward the direction of motion. Since a person lifts their legs higher at faster speeds, the acrobot's legs should pivot to an angle proportional to the swing's speed. Because the direction of motion is entirely determined by p_u, one VNHC which emulates this process is $q_a = \bar{q}_a \arctan(Ip_u)$, displayed in Figure 2. Here, $\bar{q}_a \in]0, 2Q_a/\pi]$ and $I \in \mathbb{R}$ are design parameters. This constraint does not perfectly recreate giant motion, during which the gymnast's legs are almost completely extended [1]. It instead pivots the legs partially during rotations. However, the behaviour is similar enough that this constraint will still inject energy into the acrobot. Our final VNHC is

$$h(q, p) = q_a - \bar{q}_a \arctan(Ip_u). \tag{17}$$

Recall that (q_u, p_u) denote the angle and momentum of the acrobot's torso. By Theorem 3, the constrained dynamics arising from the VNHC (17) are parameterized fully by $(q_u, p_u) \in \mathbb{S}^1 \times \mathbb{R}$. Here, (16) reduces to

$$g(q_u, p_u) = \frac{(1+c_a)(1+I^2p_u^2)p_u - m^2gl^3\bar{q}_aI(2-c_a^2)(2s_u+s_{ua})}{ml^2(3+2c_a)(1+I^2p_u^2)},$$

and the constrained dynamics (15) are

$$\begin{cases} \dot{q}_u &= \frac{(1+I^2p_u^2)p_u + m^2gl^3\bar{q}_aI(2s_u+s_{ua})(1+c_a)}{ml^2(1+I^2p_u^2)(3+2c_a)}, \\ \dot{p}_u &= -mgl(2s_u + s_{ua}), \end{cases} \tag{18}$$

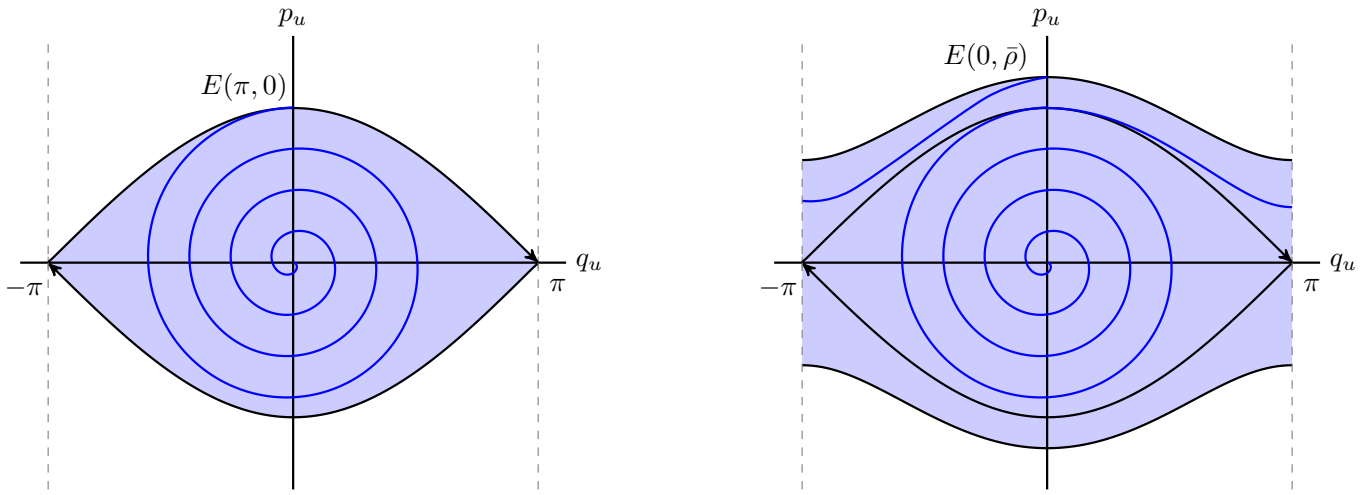

(a) The set $\mathcal{O}_1$. An orbit starting in this set (blue) will pass through the level set $E(\pi, 0)$ of the nominal pendulum.

(b) The set $\mathcal{O}_2(\rho)$. Orbits starting in this set are guaranteed to reach the level set $E(0, \rho)$ of the nominal pendulum.

Fig. 3: The sets on which the acrobot gains energy, according to Theorem 4.

subject to $q_a = \bar{q}_a \arctan(Ip_u)$.

Suppose for a moment that $I = 0$ in (17), i.e., that the legs stay fully extended. The acrobot becomes a nominal pendulum with two masses, whose total mechanical energy is

$$E(q_u, p_u) := \frac{p_u^2}{10ml^2} + 3mgl(1 - \cos(q_u)). \tag{19}$$

The upright equilibrium of this pendulum is located at $(q_u, p_u) = (\pi, 0)$. Imagine the pendulum hits the bottom of the swing arc with momentum $p_u \neq 0$. To reach the upright equilibrium, this momentum must be $p_u = \pm\sqrt{60m^2gl^3}$ because $E(\pi, 0) = E(0, \pm\sqrt{60m^2gl^3})$. If the momentum is smaller in magnitude, the acrobot will oscillate; if it is larger, the pendulum will rotate around the bar.

When the pendulum is oscillating, its state (q_u, p_u) lies in the set

$$\mathcal{O}_1 := \left\{(q_u, p_u) \in \mathbb{S}^1 \times \mathbb{R} \mid E(q_u, p_u) < E(\pi, 0)\right\}, \tag{20}$$

which is shown in Figure 3a. If for some $I \neq 0$ our VNHC injects energy into the acrobot on $\mathcal{O}_1$, and the constrained dynamics escape $\mathcal{O}_1$ in finite time, then the acrobot is guaranteed to perform giant-like motion and begin rotating around the bar.

When the pendulum is rotating with bounded momentum $|p_u| < \rho$ (for some chosen ρ), (q_u, p_u) must lie inside the rotation domain

$$\mathcal{R}(\rho) := \left\{(q_u, p_u) \in \mathbb{S}^1 \times \mathbb{R} \mid E(\pi, 0) < E(q_u, p_u) < E(0, \rho)\right\}. \tag{21}$$

Connecting the regions (20) and (21) yields the set

$$\mathcal{O}_2(\rho) := \left\{(q_u, p_u) \in \mathbb{S}^1 \times \mathbb{R} \mid E(q_u, p_u) < E(0, \rho)\right\}, \tag{22}$$

shown in Figure 3b. If the VNHC injects energy on $\mathcal{O}_2(\rho)$ for some $I \neq 0$, then the acrobot must necessarily swing up, begin rotating, and eventually rotate with a momentum of at least ρ.

Unfortunately, our VNHC does not always inject energy on $\mathcal{O}_1$ and $\mathcal{O}_2(\rho)$. If I is too large, the leg controller saturates and the body oscillates without gaining energy. Choosing I small enough guarantees the legs will synchronize properly with the body, and the acrobot will begin rotating around the bar. The following theorem provides conditions under which such an I exists.

Theorem 4: Consider the acrobot with Hamiltonian dynamics given in (6).

1) For each $m, g, l, \bar{q}_a > 0$, there exists $I^\star > 0$ such that, for all $I \in]0, I^\star]$, the VNHC (17) injects energy into the acrobot on $\mathcal{O}_1$. Moreover, almost every orbit of the constrained dynamics (18) will escape the closure of $\mathcal{O}_1$ in finite time. If instead $I \in [-I^\star, 0[$, the VNHC dissipates energy.
2) Let $C = m^2gl^3\bar{q}_a$ and define $b : \mathbb{S}^1 \times \mathbb{R}_{>0} \to \mathbb{R}$ by

$$b(\beta, \rho_0) := \frac{5C\left(\frac{C}{\bar{q}_a}\left(18s_\beta^2 + 30c_\beta(1 - c_\beta)\right) - c_\beta\rho_0^2\right)}{|\rho_0|\sqrt{\rho_0^2 - 30m^2gl^3(1 - c_\beta)}}.$$

Define $S(\rho_0) := \int_0^{2\pi} b(\sigma, \rho_0) d\sigma$. Fix $\rho > \sqrt{60m^2gl^3}$ and suppose there exists $\epsilon > 0$ so that $S(\rho_0) \geq \epsilon$ for all $\rho_0 \in \left]\sqrt{60m^2gl^3}, \rho\right]$. Then there exists $I^{\star\star} \in]0, I^\star]$ such that, for all $I \in]0, I^{\star\star}]$, the VNHC (17) injects energy into the acrobot on $\mathcal{O}_2(\rho)$. If instead $I \in [-I^{\star\star}, 0[$, the VNHC dissipates energy.

Proof: See Section VII. ∎

Notice that $\mathcal{O}_1 \subset \mathcal{O}_2(\rho)$, yet Theorem 4 considers these sets separately. This separation is advantageous because the first result holds for any positive m, g, l, and $\bar{q}_a$. In other words, the first result of Theorem 4 states that all acrobots constrained by (17) will gain enough energy to begin rotating around the bar.

For the acrobot to achieve giants with energy $E(0, \rho)$, it must satisfy the assumption on the integral of $b(\beta, \rho_0)$. The value of this integral depends on the acrobot's physical parameters. If the assumption holds, there is some control value I (which depends on ρ) for which the acrobot will achieve rotations with a momentum of at least ρ.

A. Energy Regulation

One can apply the results of Theorem 4 towards energy regulation; that is, one can stabilize oscillations or rotations by appropriately toggling between injection and dissipation VNHCs.

Oscillation Regulation: one chooses a desired oscillation angle $q_{\text{des}} \in]0, \pi[$ and, to avoid infinite switching, a hysteresis value $\delta \in [0, 1]$. Each time the orbit crosses the q_u-axis (i.e., when $p_u = 0$) or when $|q_u| = \pi$, the supervisor does the following:

- If $|q_u| < (1 - \delta)q_{\text{des}}$, enable the injection VNHC.
- If $|q_u| > (1 + \delta)q_{\text{des}}$, enable the dissipation VNHC.
- If $(1 - \delta)q_{\text{des}} \leq |q_u| \leq (1 + \delta)q_{\text{des}}$, keep the leg extended at $q_a = 0$. This can be done continously since $q_a = 0$ when $p_u = 0$.

Here one must be careful to choose δ so that $(1 + \delta)q_{\text{des}} < \pi$, otherwise a rotating acrobot will not dissipate energy.

Rotation Regulation: one chooses a desired rotation rate $p_{\text{des}} > 0$ and a hysteresis value $\delta \in [0, 1]$. Each time the orbit crosses the p_u-axis (i.e. when $q_u = 0$), the supervisor changes which VNHC is enforced as follows:

- If $|p_u| < (1 - \delta)p_{\text{des}}$, enable the injection VNHC.
- If $|p_u| > (1 + \delta)p_{\text{des}}$, enable the dissipation VNHC.
- If $(1 - \delta)p_{\text{des}} \leq |p_u| \leq (1 + \delta)p_{\text{des}}$, extend the leg fully by setting $q_a = 0$. For these simulations, we assume this can be done instantaneously.

While this method is titled "rotation regulation", it is entirely possible to choose $p_{\text{des}} < \sqrt{60m^2gl^3}$; this would stabilize an oscillation whose momentum at the bottom of the swing arc is p_{des}.

V. Simulation Results

In Section VI we will test our VNHC on a physical acrobot. This acrobot cannot be modelled by the simplified setup in Figure 1, because the torso and leg links have distributed mass. We must therefore use the more general acrobot model in Figure 4 to represent this system. Let us define

$$\begin{aligned} m_{11}(q) :=& m_a l_u^2 + 2m_a l_u l_{c_a} \cos(q_a) + m_a l_{c_a}^2 + m_u l_{c_u}^2 \\ &+ J_u + J_a, \\ m_{12}(q) :=& m_a l_{c_a}^2 + m_a l_u l_{c_a} \cos(q_a) + J_a, \\ m_{22}(q) :=& m_a l_{c_a}^2 + J_a, \end{aligned}$$

where J_u and J_a are the moments of inertia of the torso and leg links respectively. The general acrobot has inertia matrix

$$M(q) = \begin{bmatrix} m_{11}(q) & m_{12}(q) \\ m_{12}(q) & m_{22}(q) \end{bmatrix},$$

and potential function

$$V(q) = g\big(m_a l_{c_a}(1 - c_{ua}) + (m_a l_u + m_u l_{c_u})(1 - c_u)\big).$$

Recall that we defined the sets $\mathcal{O}_1$ and $\mathcal{O}_2(\rho)$ used in Theorem 4 via the mechanical energy (19) of the nominal pendulum associated with a simplified acrobot. We obtained this nominal pendulum by setting $I = 0$ in (17). The boundary between oscillations and rotations of the nominal pendulum is obtained by finding the level set E_π of the nominal energy corresponding to the upright equilibrium $(q_u, p_u) = (\pi, 0)$.

We can extend this idea to find the nominal pendulum associated with our physical acrobot, whose parameters are provided in Table I. Setting $I = 0$ in (17) for this acrobot yields the following mechanical energy of the nominal pendulum:

$$E(q_u, p_u) \approx 396.5501 p_u^2 + 0.5997(1 - \cos(q_u)).$$

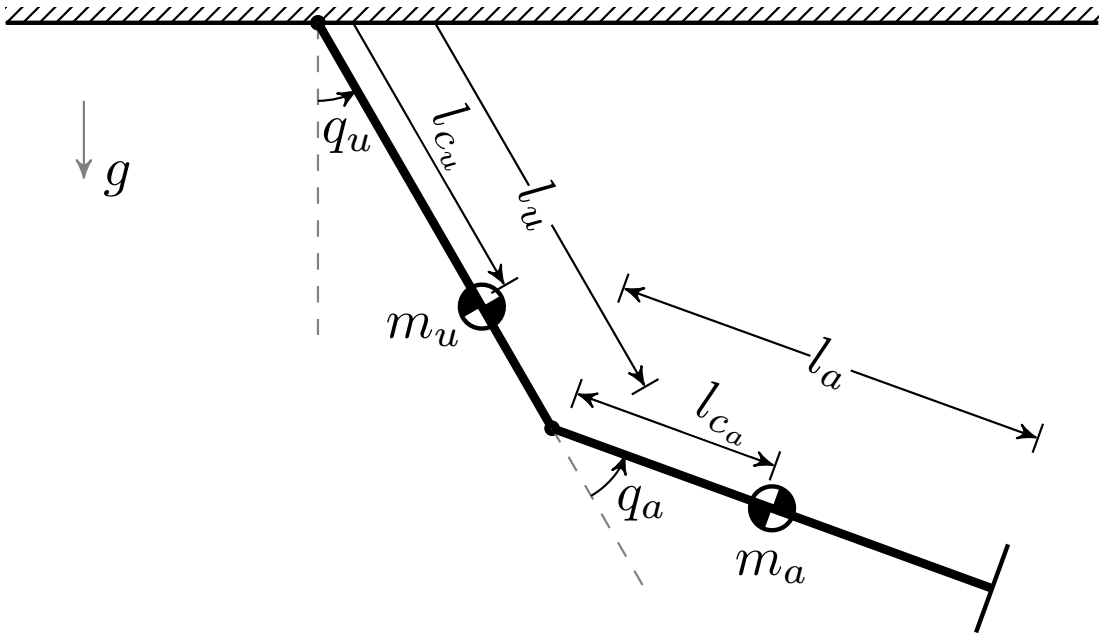

Fig. 4: The general acrobot model, represented by two weighted rods differing in both length and mass.

TABLE I: Physical parameters for the real acrobot.

m_u (kg)	m_a (kg)	l_u (m)	l_a (m)	l_{c_u} (m)	l_{c_a} (m)	J_u (kg·m^2)	J_a (kg·m^2)	g (m/s^2)
0.2112	0.1979	0.148	0.145	0.073	0.083	0.00129	0.00075	9.81

Despite the change in model, the level set E_π with energy $E(\pi, 0)$ remains the boundary between oscillations and rotations for this nominal pendulum.

We will now simulate the effects of constraining our real acrobot with the VNHC (17), thereby demonstrating that VNHCs are robust to model mismatch. According to Theorem 4, the control parameter I must be "small" for our VNHC to inject (or dissipate) energy into the simplified acrobot. Unfortunately, the Theorem does not specify how small $|I|$ must be; while we could make it arbitrarily small in simulations, we will eventually implement this VNHC on a physical testbed where $|I|$ must be large enough to overcome friction.

Setting $\bar{q}_a = 1$, we experimentally determined that $|I| = 10$ is a viable control parameter, so this is the value we will use for all simulations and experiments. In other words, our *injection VNHC* is (17) with $I = 10$ while our *dissipation VNHC* is (17) with $I = -10$.

A. Energy Injection

In simulation, we stabilized the injection VNHC for the acrobot using the controller (14). We initialized the acrobot on the constraint manifold with initial condition $(q_u, p_u) = (\pi/32, 0)$ and simulated the constrained system for 30 seconds. The resulting orbit is plotted in Figure 5.

The level set E_π with energy $E(\pi, 0)$ is outlined in black. Recall that this level set is the boundary between oscillations and rotations of the nominal pendulum. The points where the orbit exits E_π are marked with black stars, with the final departure marked by a red star. Interestingly, our choice of I is large enough that we observe significant differences between the nominal pendulum and the constrained dynamics: E_π intersects the p_u-axis at $|p_u| \approx 0.18$, yet the constrained acrobot begins rotating once it hits the p_u-axis at $|p_u| \approx 0.16$. This indicates that higher values of I enable the acrobot to gain energy faster and begin rotating sooner, so long as the actuator does not saturate.

To verify numerically that the acrobot would consistently achieve rotations, we ran a Monte-Carlo [22] simulation where we initialized the acrobot randomly inside the sublevel set

$$\left\{(q_u, p_u) \in \mathbb{S}^1 \times \mathbb{R} \mid E(q_u, p_u) \leq E\left(\frac{\pi}{32}, 0\right)\right\},$$

and measured how long it took to begin rotating. The results in Figure 6 show that the acrobot always rotated within 20–40 seconds.

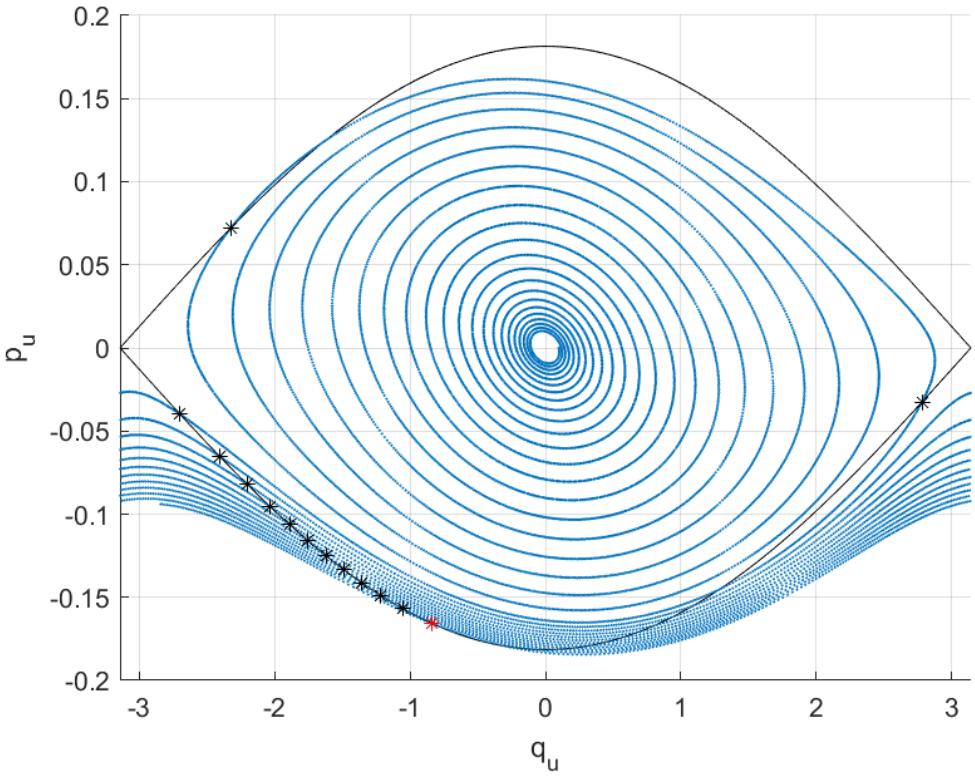

Fig. 5: A simulation of the acrobot gaining energy.

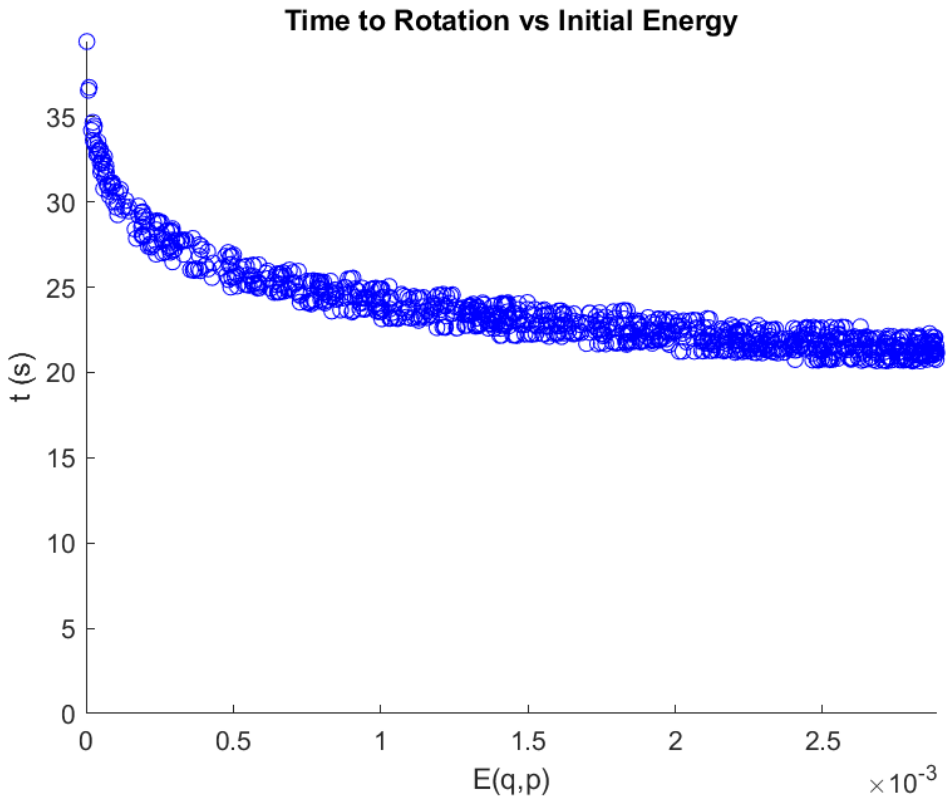

Fig. 6: Monte Carlo simulation for energy injection.

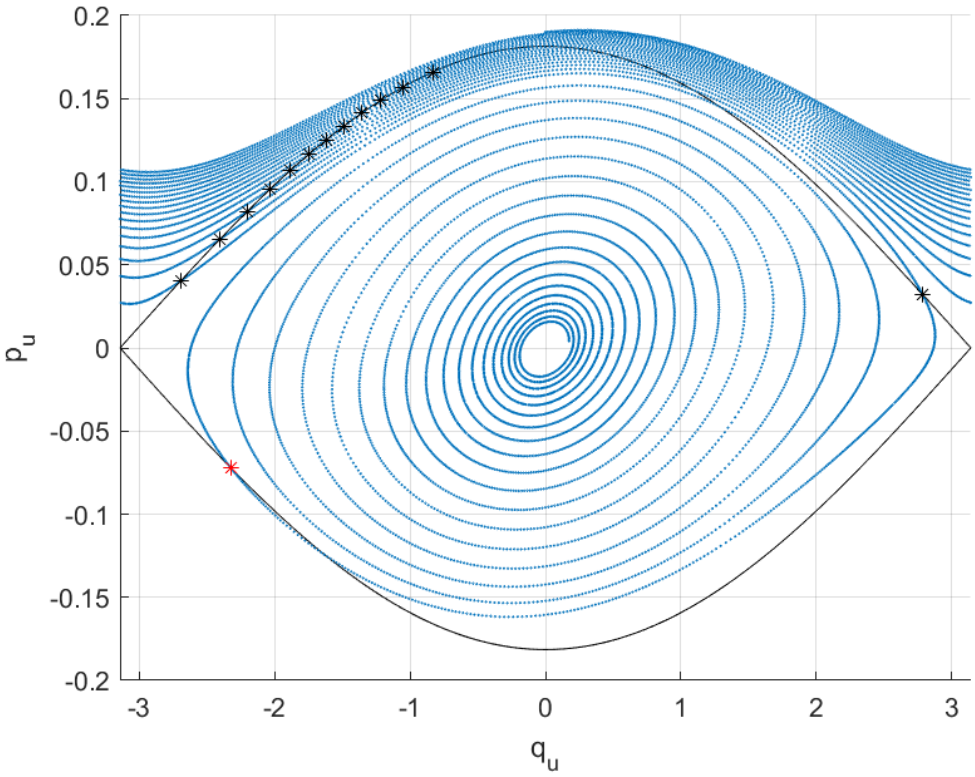

Fig. 7: A simulation of the acrobot dissipating energy.

B. Energy Dissipation

In simulation, we stabilized the dissipation VNHC and initialized the acrobot on the constraint manifold with a rotation $(q_u, p_u) = (0, 0.18)$. We simulated the constrained system for 30 seconds and plotted the resulting orbit in Figure 7. As expected, the acrobot slows down over time. We highlight the locations where the orbit crossed the set E_π by black stars, with the final crossing in red. After this final crossing, the acrobot ceased rotating and its oscillations decayed to zero.

C. Oscillation Regulation

Recall from Section IV-A that one can use a supervisor to stabilize oscillations by appropriately toggling between injection and dissipation VNHCs whenever the orbit of the acrobot crosses the q_u-axis. Figure 8 shows the supervisor stabilizing an oscillation with body angle $q_{\text{des}} = \pi/2$ and a 5% hysteresis, meaning $\delta = 0.05$. The supervisor reevaluated its choice of VNHC at each black star; the red contour corresponds to the part of the orbit where the supervisor kept the leg extended, because the oscillation was within tolerance of q_{des}. The solid black line is the desired oscillation, and the dashed black lines show the hysteresis around that orbit.

In Figure 8a the acrobot was initialized at $(q_u, p_u) = (\pi/32, 0)$; here the supervisor injected energy for most of the orbit. In Figure 8b the acrobot was initialized at the rotation $(q_u, p_u) = (0, 0.19)$; here the supervisor dissipated energy. In both cases, the supervisor stabilized the desired oscillation.

D. Rotation Regulation

One can also use a supervisor to stabilize rotations through the mechanism described in Section IV-A, where the supervisor toggles between injection and dissipation VNHCs at each crossing of the p_u-axis. Rotation regulation for the acrobot is demonstrated in Figure 9, where the supervisor stabilizes $p_{\text{des}} = 0.19$ with a 2% hysteresis $\delta = 0.02$. The supervisor evaluated its choice of VNHC at each black star. Once it was within range of p_{des} it extended the legs completely, the orbit of which is shown in red.

In Figure 9a the acrobot was initialized at the oscillation $(q_u, p_u) = (\pi/2, 0)$; here the supervisor injected energy until the orbit hit the p_u-axis near p_{des}. In Figure 9b the acrobot was initialized at the (fast) rotation $(q_u, p_u) = (0, 0.23)$; here the supervisor dissipated energy. In both cases, the desired rotation was stabilized correctly.

Note the difference in shape between the blue rotations of the dissipation VNHC and the red rotation of the nominal pendulum: the red one slows down much more near $|q_u| = \pi$. This difference arises because of the size of I: if $|I|$ were

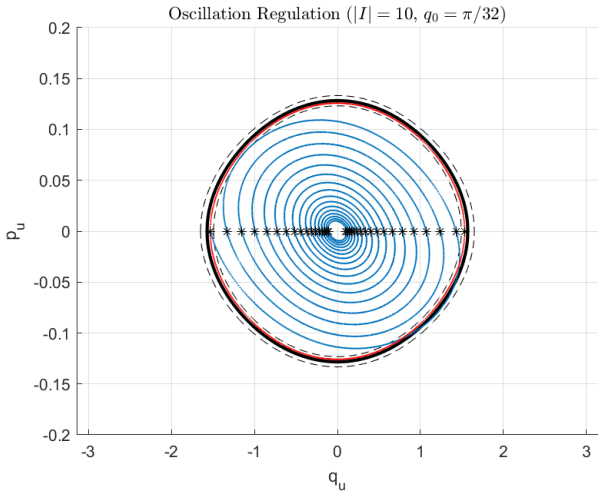

(a) Stabilizing an oscillation from below.

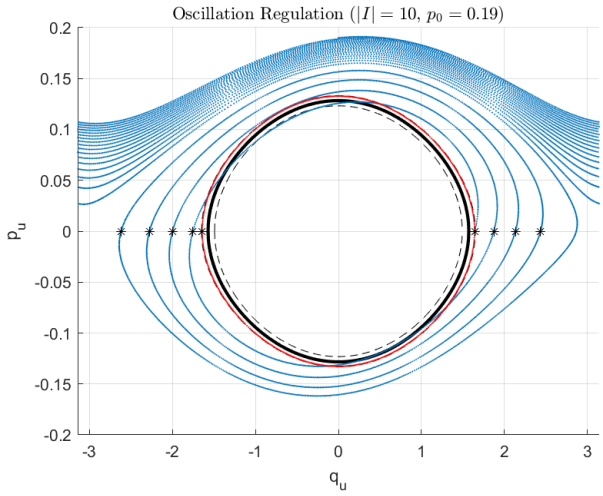

(b) Stabilizing an oscillation from above.

Fig. 8: Using a supervisor to stabilize the oscillation with peak angle $q_{\text{des}} = \pi/2$. The desired oscillation is depicted with a solid black line.

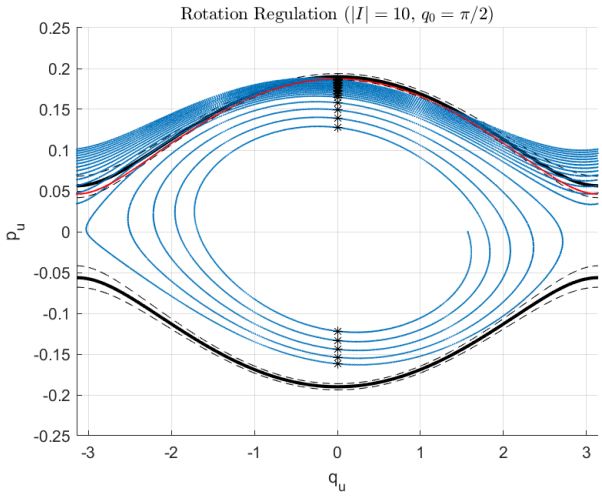

(a) Stabilizing a rotation from below.

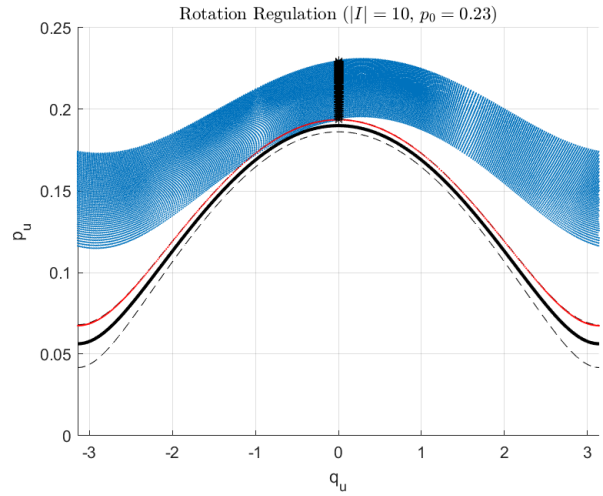

(b) Stabilizing a rotation from above.

Fig. 9: Using a supervisor to stabilize the rotation with maximal momentum $p_{\text{des}} = 0.23$. The desired rotation is depicted with a solid black line.

smaller, the blue rotations would be more similar in shape to the red one because the constrained dynamics for the dissipation VNHC would be well approximated by the nominal pendulum.

E. Summary of Results

The simulation results in this section demonstrate the energy regulation capabilities of our VNHC. We were able to stabilize both oscillations and rotations by implementing a control supervisor which toggled between injection, dissipation, and leg-extension VNHCs. In particular, these simulations indicate that our VNHC works even for acrobots whose limbs have differing masses and lengths.

VI. Physical Experiments

A. Hardware Description

In this section we will demonstrate that our VNHC is robust to friction, sensor noise, and other real-world considerations by testing it on our physical acrobot (Figure 10). This platform is called SUGAR, which stands for Simple Underactuated Gymnastics and Acrobatics Robot. Its dynamic parameters are outlined in Table I.

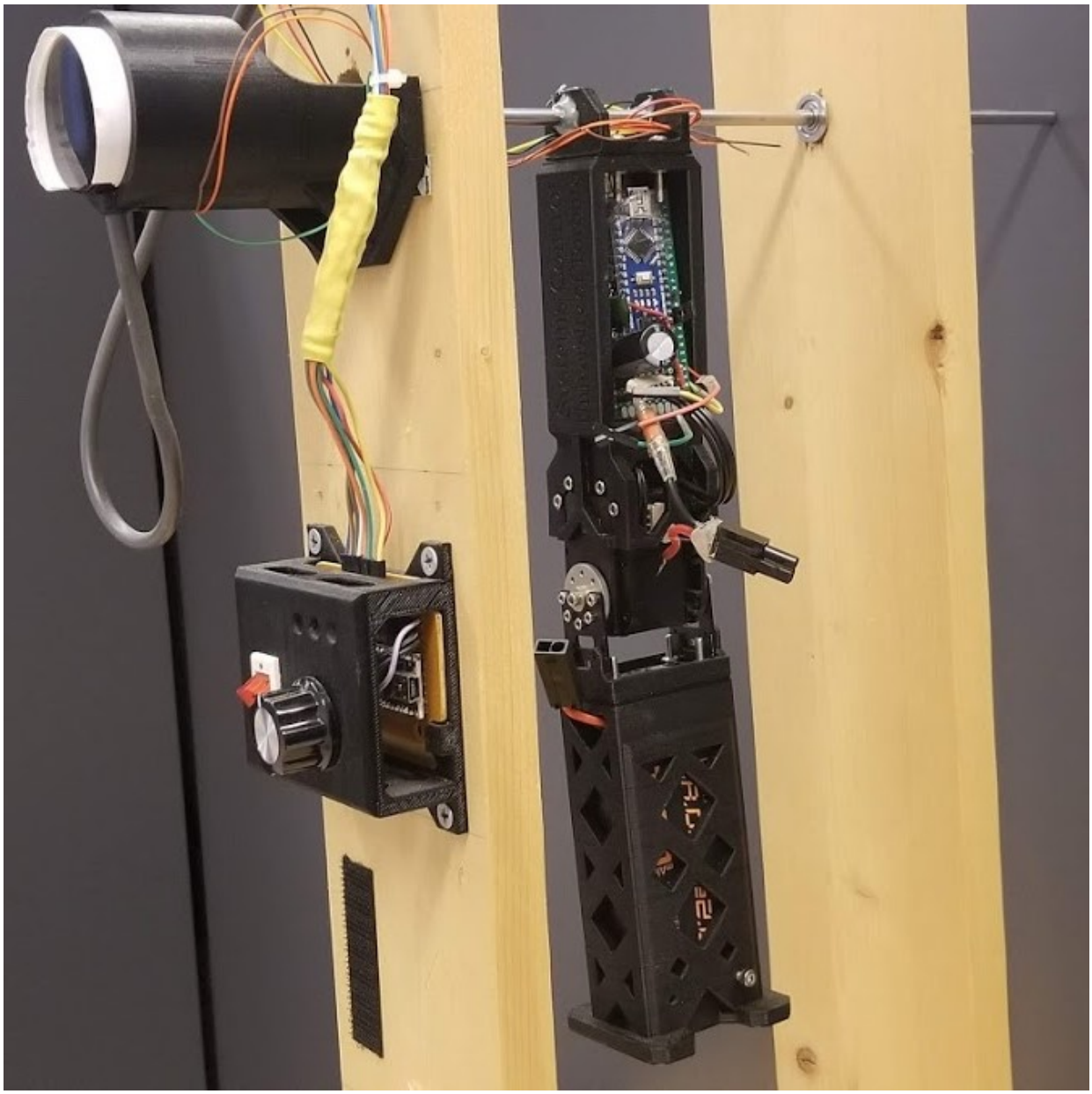

Fig. 10: SUGAR is the physical acrobot built by Wang [4].

SUGAR is comprised of two 3D-printed links: a torso and a leg. The torso houses an Arduino Nano microcontroller unit (MCU) which controls a Dynamixel RX24F servo motor between the torso and the leg. The MCU and the motor are powered by a 12V battery held in a compartment in the leg.

The torso is rigidly attached to a metal bar, which is held up by two wooden posts. On the exterior of one post is a control box with a power switch and a second Arduino Nano 328. The purpose of this control box is to read measurements from a rotary encoder connected to the metal bar, and to transmit these measurements to the MCU. The two Arduinos communicate through wires attached to a slip ring on the metal bar, and the signals are transmitted via I2C. The control box also provides a USB interface which allows the user to read the data from the acrobot in real time.

The rotary encoder directly measures q_u, and the Dynamixel servo motor provides measurements of q_a. However, there are no sensors measuring the velocity $\dot{q}$, which means we cannot directly evaluate p_u and p_a. To resolve this issue, the MCU estimates $\dot{q}$ by applying a washout filter to sequential measurements of q. We then compute $p = M(q)\dot{q}$ for use in the VNHC controller.

Communication between the Arduinos restricts the sampling rate of p to 500Hz. This low sampling rate results in a noisy momentum signal which suffers from noticeable phase lag. This also rate-limits the control signal to 500Hz, which impacts any control implementation.

Finally, The Dynamixel servo motor does not have a torque control mode; instead, we can assign the servo setpoint at

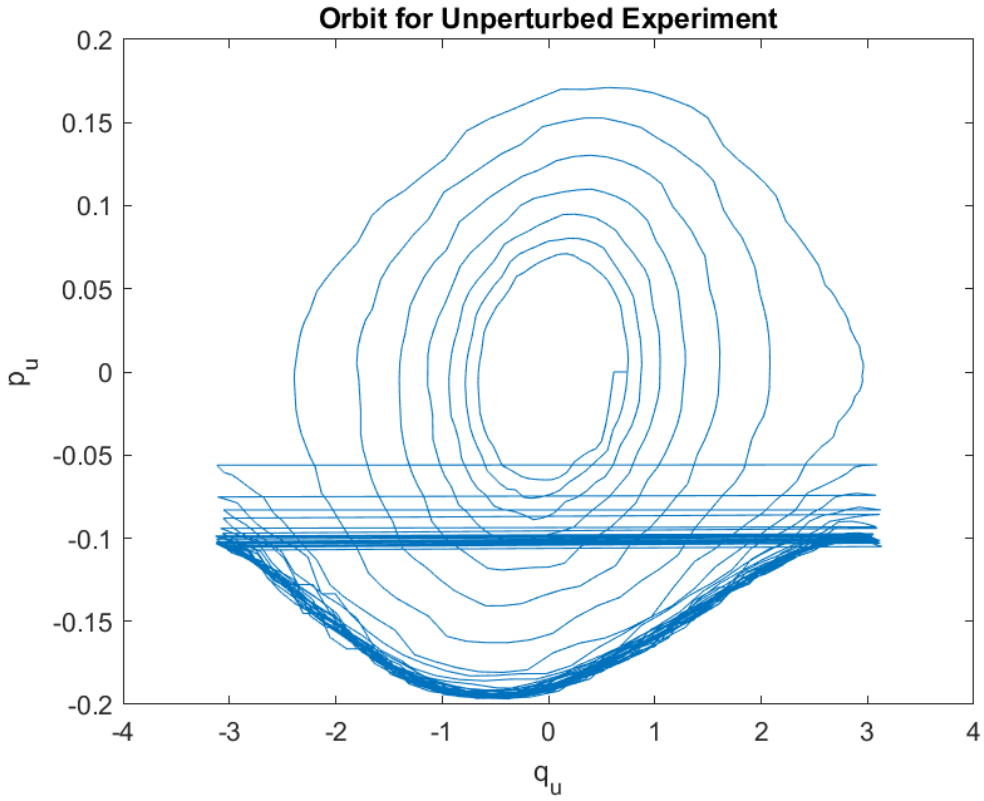

Fig. 11: Baseline Test: SUGAR's baseline energy injection orbit.

iteration $k \in \mathbb{Z}_{>0}$ via $q_a^k = \arctan(Ip_u^{k-1})$. This negatively affects the stabilization to the constraint manifold because we are introducing timing errors from the servo's built-in PID controller.

B. Experimental Results

We performed the following tests on SUGAR with the energy injection VNHC.

1) **Baseline Test:** we initialized SUGAR at $(q_u, p_u) \approx (\pi/8, 0)$. The resulting orbit in Figure 11 shows that SUGAR clearly gaining energy over time. Its motion looks similar to that of the energy injection simulation (Figure 5), though its energy gain ceases once it reaches a rotation with energy $E(0, 0.195)$. The energy gain likely ceases because of friction at the pivot, which was not modelled in simulation.
2) **Perturbation Test 1:** we initialized SUGAR at $(q_u, p_u) \approx (\pi, 0)$, let it run for 15 seconds, then introduced a rod as it passed through the bottom of its arc. This caused a collision which stopped SUGAR in its tracks, at which point we immediately removed the rod so SUGAR could continue unperturbed. The resulting orbit is shown in Figure 12. The blue rotation curve corresponds to the orbit before the disturbance, while the red spiral confirms that SUGAR begins oscillating after it was stopped. After the collision, SUGAR gains energy and eventually starts rotating again.
3) **Perturbation Test 2:** to see how SUGAR responds when pushed, we allowed it to rotate unperturbed for 15 seconds and then pushed it in its direction of motion. The orbit in Figure 13a shows that SUGAR, when pushed, rotates with energy $E(0, -0.22)$, but then slows down until it reaches a rotation with energy $E(0, -0.195)$. We repeated this test by pushing SUGAR against its direction of motion. The orbit in Figure 13b demonstrates that it readily changes direction, and quickly achieves its maximum speed with energy $E(0, 0.195)$.

In simulation, the acrobot was able to gain energy even when initialized with energy $E(q_u, p_u) > E(0, 0.195)$. The baseline and push tests suggest that our VNHC injects energy into SUGAR only on $\mathcal{O}_2(0.195)$. This difference between simulation and implementation is likely due to friction, as well as timing errors incurred by the PID controller in the servo motor.

We had hoped to show experimental results for dissipation and oscillation/rotation regulation. Unfortunately the Dynamixel RX24F servo motor broke before we could perform these experiments. These motors are no longer in production at the time of writing this article, so SUGAR has been retired from service.

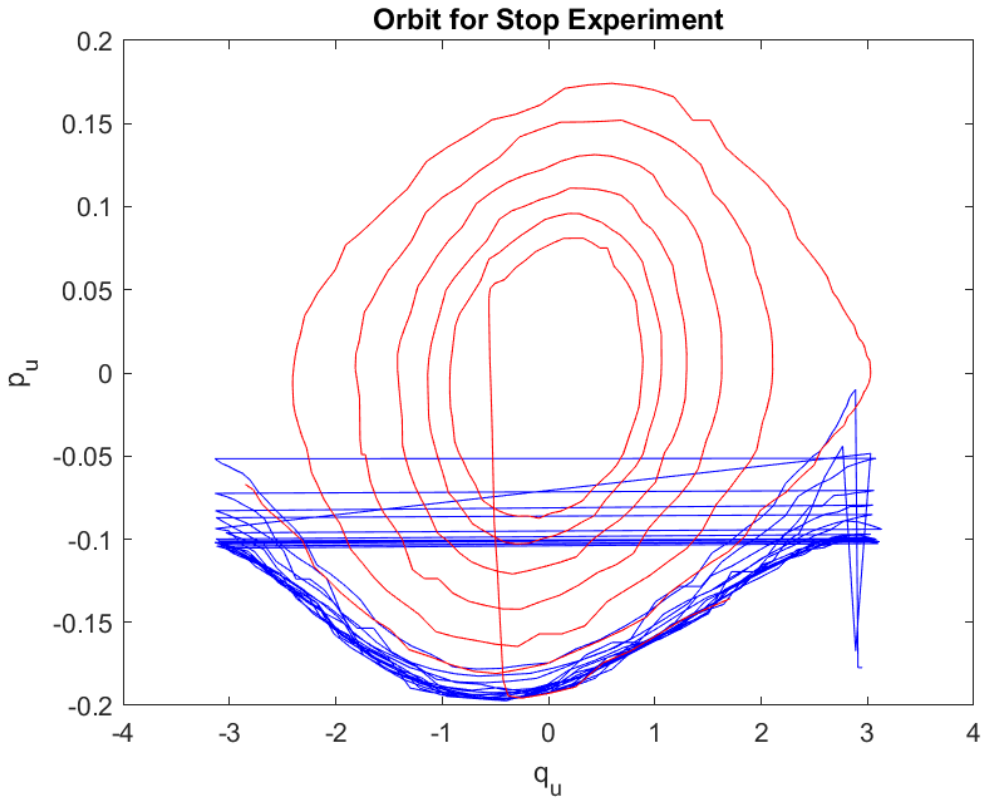

Fig. 12: Perturbation Test 1: SUGAR's orbit before (blue) and after (red) stopping.

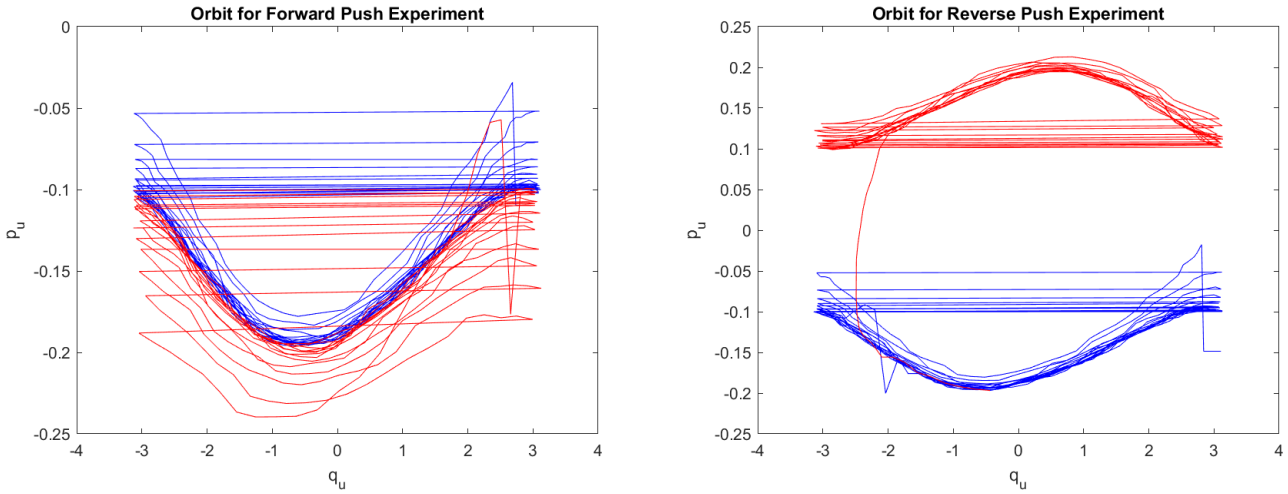

(a) The forwards push test.

(b) The reverse push test.

Fig. 13: Perturbation Test 2: SUGAR's orbit before (blue) and after (red) pushing.

C. Summary of Results

We performed three tests on SUGAR: a baseline energy injection test, a stop test, and a push test. These experiments demonstrate that VNHC-based energy injection is robust to significant model mismatch, friction, sensor noise, discretized control implementation, rate-limited measurement and control signals, and dramatic external disturbances.

VII. Proof of Theorem 4

In this section we prove Theorem 4, which claims the acrobot gains/loses energy on $\mathcal{O}_1$ and $\mathcal{O}_2(\rho)$. These are the sublevel sets (20) and (22) of the nominal pendulum's energy $E(q_u, p_u)$ defined in (19).

Here is fundamental idea behind this proof: using a procedure devised by Mohammadi *et al.* [23], on certain subsets $D \subset \mathbb{S}^1 \times \mathbb{R}$ one can find a diffeomorphism $T(q_u, p_u) = (r, \theta)$ into pseudo-polar coordinates adapted to level sets of $E(q_u, p_u)$. That is, when $I = 0$ in (17), the pseudo-radius r chooses a level set of E and the pseudo-angle θ chooses a point on that level set. We can formally show that r increases "on average", which means E also increases on average and the constrained dynamics are gaining energy on D. We formalize this idea in the following lemma.

Lemma 2: Consider the simplified acrobot (6) constrained by the VNHC (17), whose constrained dynamics are (18). Let $D \subset \mathbb{S}^1 \times \mathbb{R}$ be open and let $]\underline{r}, \overline{r}[\subset \mathbb{R}_{>0}$. Suppose there exists a diffeomorphism

$$\begin{aligned} T : D &\to]\underline{r}, \overline{r}[\times \mathbb{S}^1 \\ (q_u, p_u) &\mapsto (r, \theta), \end{aligned}$$

into pseudo-polar coordinates adapted to level sets of $E(q_u, p_u)$, satisfying $\dot{r} \equiv 0$ and $\dot{\theta} > 0$ when $I = 0$. Let $g(\theta, r, I) = \dot{r}/\dot{\theta}$ and assume that $(\partial g/\partial r)(\theta, r, 0) \equiv 0$. Assume $b(\theta, r_0) = (\partial g/\partial I)(\theta, r_0, 0)$ is 2π-periodic in θ for any fixed r_0, and that there exists $\epsilon > 0$ such that $S(r_0) := \int_0^{2\pi} b(\sigma, r_0) d\sigma \geq \epsilon$ for all $r_0 \in]\underline{r}, \overline{r}[$. Then there exists $I^\star > 0$ small enough that the constrained dynamics gain energy on D for all $I \in]0, I^\star]$, and lose energy on D for all $I \in [-I^\star, 0[$.

Proof: Since $\dot{\theta} > 0$ when $I = 0$ and the constrained dynamics in (r, θ) coordinates are continuous in I, there exists $I_1 > 0$ small enough that $\dot{\theta} > 0$ for all $I \in [-I_1, I_1]$. Hence, we can perform a time reparameterization $t = t(\theta)$ to get a time-scaled pseudo-radius $\hat{r}(\theta) := r(t(\theta))$. This reduces the system $(\dot{r}, \dot{\theta})$ into the scalar time-varying ODE

$$\begin{cases} \hat{r}' = \frac{\dot{r}}{\dot{\theta}}\Big|_{r=\hat{r}(\theta)} = g(\theta, \hat{r}, I), \\ \hat{r}(0) = r_0, \end{cases} \tag{23}$$

where θ now represents time, the prime denotes differentiation by θ, and $r_0 \in]\underline{r}, \overline{r}[$ is the initial condition.

Let $\hat{r}(\theta, r_0, I)$ be the solution to (23). Taking the Taylor expansion of this solution around $I = 0$ we get $\hat{r}(\theta, r_0, I) = \hat{r}(\theta, r_0, 0) + I\hat{r}_1(\theta, r_0) + R(\theta, r_0, I)$. Note that $\hat{r}(\theta, r_0, 0) \equiv r_0$ because $g(\theta, \hat{r}, 0) \equiv 0$. The function $\hat{r}_1(\theta, r_0)$ is the solution to

$$\begin{cases} \hat{r}_1' = \frac{\partial g}{\partial \hat{r}}(\theta, r_0, 0)\hat{r}_1 + b(\theta, r_0), \\ \hat{r}_1(0) = 0, \end{cases} \tag{24}$$

and the remainder term $R(\theta, r_0, I)$ is $O(I^2)$.

Our assumption that $(\partial g/\partial r)(\theta, r_0, 0) \equiv 0$ means that $(\partial g/\partial \hat{r})(\theta, r_0, 0) \equiv 0$. The solution of (24) can therefore be obtained by quadrature, giving $\hat{r}_1(\theta, r_0) = \int_0^\theta b(\sigma, r_0) d\sigma$. Since and $\dot{\theta} > 0$ and $b(\theta, r_0)$ is 2π-periodic in θ, there is a well-defined Poincaré map describing how $\hat{r}$ changes each time θ increases by 2π. This map is

$$P :]\underline{r}, \overline{r}[\to \mathbb{R}_{\geq 0} \tag{25}$$

$$r_0 \mapsto \hat{r}(2\pi, r_0, I), \tag{26}$$

which expands to $P(r_0) = r_0 + IS(r_0) + R(2\pi, r_0, I)$. In other words, we can understand the evolution of $\hat{r}$ by studying the dynamics of the discrete-time system

$$r_{n+1} = P(r_n) = r_n + IS(r_n) + R(2\pi, r_n, I), \tag{27}$$

with initial condition r_0. Here, r_n corresponds to the distance along the line segment $L :=]\underline{r}, \overline{r}[\times \{0\}$ when an orbit of (r, θ) hits L for the the n^{th} time, assuming the acrobot was initialized at $(r, \theta) = (r_0, 0)$.

If $r_n \notin]\underline{r}, \overline{r}[$, the orbit in (q_u, p_u) coordinates must have departed D. Proving the constrained dynamics gain energy on D is therefore equivalent to finding $N \in \mathbb{Z}_{>0}$ where $\hat{r}_n \geq \overline{r}$ for all $n \geq N$. Using a perturbation analysis (see Khalil [24, Theorem 10.1]), we know there exists some $I_2 \in]0, I_1]$ and $\kappa > 0$ such that $|R(2\pi, r_n, I)| \leq \kappa I^2$ for all $I \in [-I_2, I_2]$. Taking this fact alongside the assumption that $S(r_0) \geq \epsilon$, we find a lower bound $r_{n+1} \geq r_n + I\epsilon - \kappa I^2$. Choosing $\gamma > 0$ and $I^\star \in]0, I_2]$ small enough makes $I\epsilon - \kappa I^2 \geq \gamma$ for all $I \in]0, I^\star]$. Therefore, $r_n \geq r_0 + n\gamma$, so all solutions of (27) eventually flow past $\overline{r}$. We conclude that, for $I \in]0, I^\star]$, the constrained dynamics gain energy on D.

Changing the sign of I changes the direction of all the above inequalites, so that $r_n \leq r_0 - n\gamma$. In this case all orbits of (27) flow below $\underline{r}$, i.e., the constrained dynamics lose energy on D. ■

A. Energy Gain on $\mathcal{O}_1$

To prove the first part of Theorem 4, we begin by using the procedure from [23] to find pseudo-polar coordinates (adapted to level sets of E) on the punctured open set $\mathcal{O}_1 \backslash \{(0,0)\} \subset \mathbb{S}^1 \times \mathbb{R}$. The resulting coordinate transformation is

$$r = \arccos\left(\cos(q_u) - \frac{p_u^2}{30m^2gl^3}\right), \tag{28}$$

$$\theta = \operatorname{arctan}_2\left(-\operatorname{sgn}(p_u)\sqrt{1-\frac{q_u^2}{r^2}}, \frac{q_u}{r}\right)\Bigg|_{r=r(q_u,p_u)}, \tag{29}$$

where $(r,\theta) \in]0,\pi[\times\mathbb{S}^1$. One can verify that the inverse to this transformation is

$$\begin{aligned} q_u &= rc_\theta, \\ p_u &= -\operatorname{sgn}(s_\theta)\sqrt{30m^2gl^3\cos(rc_\theta - c_r)}, \end{aligned}$$

where for shorthand we write $c_\theta := \cos(\theta)$, $s_\theta := \sin(\theta)$, $c_r := \cos(r)$, and $s_r := \sin(r)$. We now verify these pseudo-polar coordinates satisfy the requirements of Lemma 2.

When $I = 0$ we have $\dot{r} = 0$ and

$$\dot{\theta} = \sqrt{\frac{6g}{5l}}\sqrt{\frac{\cos(rc_\theta) - c_r}{r^2 s_\theta^2}}. \tag{30}$$

Note that (30) has removable singularities at $\theta \in \{0,\pi\}$. Taking the limit as θ approaches these points yields

$$\lim_{\theta\to 0}\dot{\theta} = \lim_{\theta\to\pi}\dot{\theta} = \sqrt{\frac{6gs_r}{10lr}}, \tag{31}$$

which is smooth and well-defined for all $r \in]0,\pi[$. From (30)–(31), one can verify that $\dot{\theta} > 0$ when $I = 0$. Defining $g(\theta, r, I) = \dot{r}/\dot{\theta}$, MATLAB symbolic computations confirm that $(\partial g/\partial r)(\theta, r, 0) \equiv 0$ as required.

Next we compute $b(\theta, r_0) := (\partial g/\partial I)(\theta, r_0, 0) = Ka(\theta, r_0)$, where

$$\begin{aligned} K &:= \frac{\bar{q}_a\sqrt{30m^2gl^3}}{15}, \\ a(\theta, r_0) &:= \frac{r_0|s_\theta|\left(5c_{r_0}\cos(r_0c_\theta) - 8\cos(r_0c_\theta)^2 + 3\right)}{s_{r_0}\sqrt{\cos(r_0c_\theta) - c_{r_0}}}. \end{aligned}$$

Notice that K is a positive constant which depends only on m, g, l, and $\bar{q}_a$, while $a(\theta, r_0)$ is adimensional and 2π-periodic in θ. This means that there exists $\epsilon > 0$ such that $S(r_0) := \int_0^{2\pi} b(\sigma, r_0)d\sigma \geq \epsilon$ if and only if there exists $\delta > 0$ such that $Q(r_0) := \int_0^{2\pi} a(\sigma, r_0)d\sigma \geq \delta$. Since $a(\theta, r_0)$ is adimensional, we can numerically compute $Q(r_0)$ once for all acrobots. The plot of $Q(r_0)$ when $r_0 \in [10^{-10}, \pi - 10^{-3}]$ is shown in Figure 14. We see that it is strictly positive and monotonically increasing, with an asymptote at $r_0 = \pi$. Simulations with smaller r_0 result in an infinite integral error due to a division by zero, yet we believe the $Q(r_0)$ is in fact positive for all $r_0 \in]0,\pi[$.

Unfortunately there is no $\delta > 0$ such that $Q(r_0) \geq \delta$ everywhere on $]0,\pi[$, though such a δ does exist on $]\omega,\pi[$ for each fixed $\omega > 0$. This means all conditions of Lemma 2 are satisfied on the annulus

$$D_\omega = \mathcal{O}_1 \backslash \{(q_u, p_u) \in \mathbb{S}^1 \times \mathbb{R} \mid E(q_u, p_u) \leq E(\omega, 0)\}.$$

Therefore, for each $\omega \in]0,\pi[$ there exists some $I_1(\omega) > 0$ such that the acrobot gains/loses energy everywhere on D_ω. To prove energy gain on all of $\mathcal{O}_1$, we will show the origin is a repeller so that all orbits near the origin flow away from the origin into D_ω (for small enough ω) and continue gaining energy thereafter.

Recall the discrete-time pseudo-radius dynamics (27) from the proof of Lemma 2. To prove the origin is a repeller, we need simply prove the linearization of (27) is greater than 1 at $r_0 = 0$. This linearization yields

$$P'(0) = 1 + IKQ'(0) + R'(2\pi, 0, I),$$

where the prime now denotes differentiation with respect to r. MATLAB symbolic computations reveal that

$$Q'(0) = \int_0^\pi \lim_{r_0\to 0^+}\frac{\partial a}{\partial r}(\sigma, r_0)d\sigma = \frac{\pi}{2\sqrt{2}} > 0.$$

Since $R(2\pi, 0, I)$ is $O(I^2)$, so is $R'(2\pi, 0, I)$. Hence, it can be written in the form $I^2\tilde{R}(I)$ where $\tilde{R}(I)$ is smooth and zero at $I = 0$. Thus, there exists $I_0 > 0$ such that $IKQ'(0) + I^2\tilde{R}(I) > 0$ for all $I \in]0, I_0]$, which implies $P'(0) > 1$. The origin is therefore a repeller, which means there exists some (unknown) $\mu > 0$ where $]0,\mu]$ is negatively invariant for (27), and all solutions in this interval flow through $r = \mu$. Hence, all orbits in $\mathcal{O}_1$ near the origin will gain energy up to $E(\mu, 0)$.

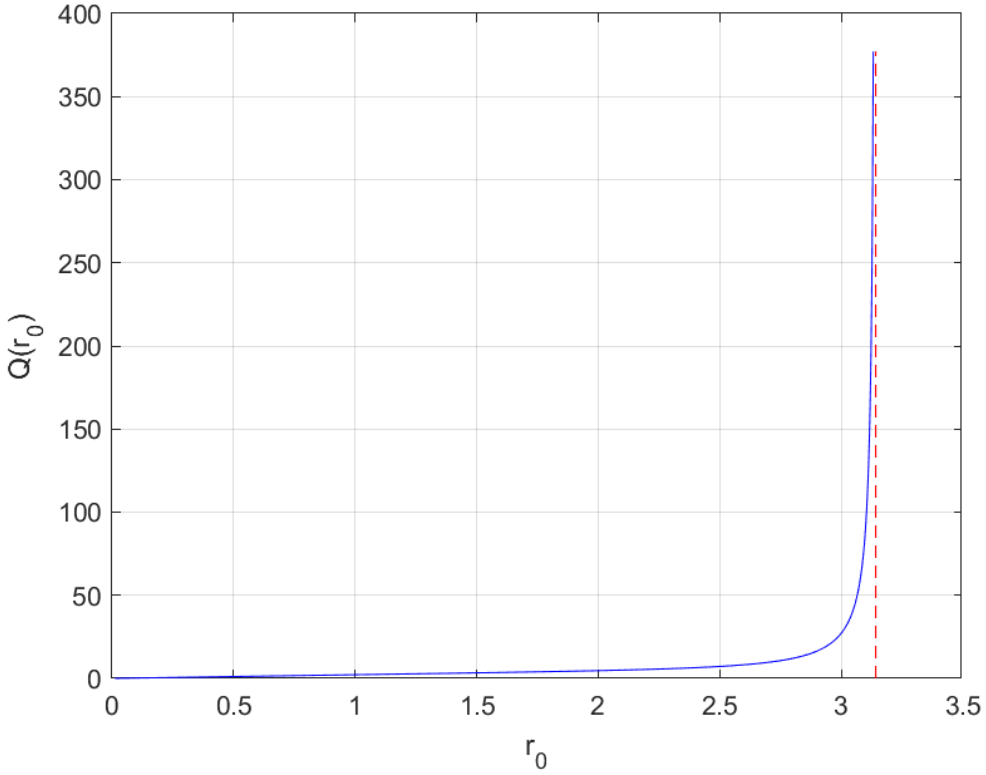

Fig. 14: The plot of $Q(r_0)$.

Since there exists $I_1(\mu)$ so that the acrobot gains energy on D_μ, taking $I^\star = \min\{I_0, I_1(\mu)\}$ means the acrobot will gain energy on $\mathcal{O}_1$ for each $I \in]0, I^\star]$. If $I < 0$, then $P'(0) < 1$ and the origin is an asymptotically stable equilibrium. Since the acrobot now loses energy on D_μ, it also loses energy on $\mathcal{O}_1$ for $I \in [-I^\star, 0[$.

We have proved that any acrobot constrained by our VNHC (17) gains/loses energy on $\mathcal{O}_1$. We must now confirm that the acrobot will start rotating: the definition of energy gain states that all orbits initialized in $\mathcal{O}_1$ will escape compact subsets of $\mathcal{O}_1$ in finite time, which is not enough to conclude that these orbits will also escape the boundary of $\mathcal{O}_1$ in finite time.

Let E_π be the level set with energy $E(\pi, 0)$, which forms the boundary of $\mathcal{O}_1$. Define $\bar{\mathcal{O}}_1 = \mathcal{O}_1 \cup E_\pi$ to be the closure of $\mathcal{O}_1$. An orbit of the acrobot will only begin rotating if it escapes $\bar{\mathcal{O}}_1$ by crossing through E_π, and eventually remains outside this set.

Taking the Jacobian of the constrained dynamics (18) at the upright equilibrium $(q_u, p_u) = (\pi, 0)$ yields

$$J = \begin{bmatrix} -\frac{6mgl\bar{q}_a I}{5} & \frac{1-2m^2gl^3\bar{q}_a^2 I^2}{5ml^2} \\ 3mgl & mgl\bar{q}_a I \end{bmatrix},$$

which has characteristic polynomial

$$\det(\lambda I_2 - J) = \lambda^2 + \frac{mgl\bar{q}_a I}{5}\lambda - 3g.$$

By Descartes' rule of signs, this polynomial always has exactly one root with positive real part. The equilibrium $(\pi, 0)$ is therefore unstable, so the stable manifold Π^+ of initial conditions converging to $(\pi, 0)$ is one-dimensional, and hence is of measure zero in $\mathbb{S}^1 \times \mathbb{R}$.

Using $x(t) := (q_u(t), p_u(t))$ as shorthand, let $x(0) \in \mathcal{O}_1$ be a nonzero initial condition of the acrobot. Suppose by way of contradiction that the orbit $x(\mathbb{R})$ is confined within $\bar{\mathcal{O}}_1$, and does not exit through E_π into the rotation zone. Since $\bar{\mathcal{O}}_1$ is compact, the Birkhoff Theorem [25] implies:

- The positive limit set L_+ of $x(t)$ is non-empty, compact, and invariant.
- The solution $x(t)$ asymptotically tends to L_+.

Since the acrobot gains energy on $\mathcal{O}_1$, the positive limit set of $x(t)$ must be the largest invariant subset of E_π. Taking the limit as $r \to \pi$ of (30)–(31), we get $\dot{\theta} \geq 0$ on E_π with equality if and only if $\theta \in \{0, \pi\}$. Thus, the largest invariant subset of E_π is either the upright equilibrium $\{(\pi, 0)\}$ or E_π itself.

Taking the derivative of $E(q_u, p_u)$ at the p_u-axis yields $\dot{E}(0, p_u) = g/(5l)\sin(q_a)p_u$. This is non-zero on E_π, so E_π is not invariant and the positive limit set of $x(t)$ must be the set $\{(\pi, 0)\}$. Hence, $x(t)$ converges to $(\pi, 0)$, so $x(0) \in \Pi^+$. Since Π^+ is a set of measure zero in $\mathbb{S}^1 \times \mathbb{R}$, almost every orbit initialized in $\mathcal{O}_1$ must escape at least once through E_π into the rotation domain. Moreover, almost every orbit must eventually remain outside $\bar{\mathcal{O}}_1$. If not, the positive limit set would once again be E_π; by the same argument as above, that orbit would be in Π^+.

We conclude that almost all orbits beginning in $\mathcal{O}_1$ will, in finite time, escape the closure of $\mathcal{O}_1$ and remain in the rotation domain forever after.

B. Energy Gain on $\mathcal{O}_2(\rho)$

Since $\mathcal{O}_2(\rho) = \bar{\mathcal{O}}_1 \cup \mathcal{R}(\rho)$ (where $\mathcal{R}(\rho)$ is the rotation domain defined in (21)), and since all orbits escape $\bar{\mathcal{O}}_1$ in finite time, we need simply prove energy gain on $\mathcal{R}(\rho)$ to prove energy gain on $\mathcal{O}_2(\rho)$. We separate $\mathcal{R}(\rho)$ into its two distinct connected components: $\mathcal{R}^+(\rho)$, the set of rotations with $p_u > 0$; and $\mathcal{R}^-(\rho)$, the set of rotations with $p_u < 0$. We take the domain of interest for Lemma 2 to be $D \in \{\mathcal{R}^+(\rho), \mathcal{R}^-(\rho)\}$.

We now apply the method described in [23] to find pseudo-polar coordinates adapted to rotations. These coordinates are

$$r = \sqrt{p_u^2 + 30m^2gl^3(1 - c_u)}, \tag{32}$$

$$\theta = \alpha(D)q_u \tag{33}$$

where $(r, \theta) \in]\sqrt{60m^2gl^3}, \rho[\times\mathbb{S}^1$, and $\alpha(D) = 1$ if $D = \mathcal{R}^+(\rho)$ or -1 if $D = \mathcal{R}^-(\rho)$. The inverse of this transformation is

$$q_u = \alpha(D)\theta,$$
$$p_u = \alpha(D)\sqrt{r^2 - 30m^2gl^3(1 - c_\theta)}.$$

In computing the constrained dynamics in (r, θ) coordinates and setting $I = 0$, we find that $\dot{r} \equiv 0$ and

$$\dot{\theta} = \frac{1}{5ml^2}\sqrt{r^2 - 30m^2gl^3(1 - c_\theta)},$$

which is strictly positive as required. Defining $g(\theta, r, I) = \dot{r}/\dot{\theta}$, symbolic computations also confirm that $(\partial g/\partial r)(\theta, r, 0) \equiv 0$. The function $b(\theta, r_0) = (\partial g/\partial I)(\theta, r_0, 0)$ is given in the statement of Theorem 4, and by assumption we have $S(r_0) \geq \epsilon$ on $]\sqrt{60m^2gl^3}, \rho[$.

All requirements of Lemma 2 are satisfied, so there exists a control parameter $I_2(\rho) > 0$ whereby the acrobot gains energy on both $\mathcal{R}^+(\rho)$ and $\mathcal{R}^-(\rho)$ for each $I \in]0, I_2(\rho)]$. Let $I_1^\star$ be the value we found for $\mathcal{O}_1$ in Section VII-A, and let $I^{\star\star} = \min\{I_1^\star, I_2(\rho)\}$. Then the acrobot gains/loses energy on $\mathcal{O}_2(\rho)$ for each $I \in]0, I^{\star\star}]$. If instead $I \in [-I^{\star\star}, 0[$, the acrobot dissipates energy on $\mathcal{O}_2(\rho)$.

This completes the proof of Theorem 4.

VIII. Conclusion

In this article we applied the framework of virtual nonholonomic constraints on the acrobot, and designed a constraint which emulates giant motion from gymnastics. We proved this constraint will inject energy into the simplified acrobot whose limbs are massless rods of equal length, with equal masses at the tips. We then performed simulations and physical experiments on a real acrobot robot. These demonstrated that virtual nonholonomic constraints are capable of injecting and dissipating energy in a robust manner, all while producing realistic biologically-inspired motion.

References

[1] P. E. Pidcoe, "The biomechanics principles behind training giant swings," Online, Virginia Commonwealth University, Richmond, VA, USA, August 2005, accessed 11 September 2020. https://usagym.org/pages/home/publications/technique/2005/8/giant.pdf.

[2] V. Sevrez, E. Berton, G. Rao, and R. J. Bootsma, "Regulation of pendulum length as a control mechanism in performing the backward giant circle in gymnastics," *Human Movement Science*, vol. 28, no. 2, pp. 250 – 262, March 2009.

[3] J. Hauser and R. Murray, "Nonlinear controllers for non-integrable systems: the acrobot example," in *1990 American Control Conference*. San Diego, USA: IEEE, May 1990.

[4] X. Wang, "Motion control of a gymnastics robot using virtual holonomic constraints," Master's thesis, University of Toronto, 2016.

[5] E. Papadopoulos and G. Papadopoulos, "A novel energy pumping strategy for robotic swinging," in *2009 17th Mediterranean Conference on Control and Automation*. Thessaloniki, Greece: IEEE, June 2009.

[6] T. Henmi, M. Chujo, Y. Ohta, and M. Deng, "Reproduction of swing-up and giant swing motion of acrobot based on a technique of the horizontal bar gymnast," in *Proceedings of the 11th World Congress on Intelligent Control and Automation*. Shenyang, China: IEEE, June 2014.

[7] X. Zhang, H. Cheng, Y. Zhao, and B. Gao, "The dynamical servo control problem for the acrobot based on virtual constraints approach," in *The 2009 IEEE/RSJ International Conference on Intelligent Robots and Systems*. St. Louis, USA: IEEE, October 2009.

[8] K. Ono, K. Yamamoto, and A. Imadu, "Control of giant swing motion of a two-link horizontal bar gymnastic robot," *Advanced Robotics*, vol. 15, no. 4, pp. 449 – 465, 2001.

[9] J. Horn, A. Mohammadi, K. Hamed, and R. Gregg, "Hybrid zero dynamics of bipedal robots under nonholonomic virtual constraints," *IEEE Control Systems Letters*, vol. 3, no. 2, pp. 386 – 391, April 2019.

[10] T. Takubo, H. Arai, and K. Tanie, "Virtual nonholonomic constraint for human-robot cooperation in 3-d space," in *2000 IEEE/RSJ International Conference on Intelligent Robots and Systems*. Takamatsu, Japan: IEEE, October 2000.
[11] S. Shibata and T. Murakami, "Psd based virtual nonholonomic constraint for human interaction of redundant manipulator," in *Proceedings of the 2004 IEEE International Conference on Control Applications*. Taipei,Taiwan: IEEE, September 2004.
[12] J. D. Castro-Díaz, P. Sánchez-Sánchez, A. Gutiérrez-Giles, M. Arteaga-Pérez, and J. Pliego-Jiménez, "Experimental results for haptic interaction with virtual holonomic and nonholonomic constraints," *IEEE Access*, vol. 8, pp. 120 959 – 120 973, July 2020.
[13] S. Vozar, Z. Chen, P. Kazanzides, and L. L. Whitcomb, "Preliminary study of virtual nonholonomic constraints for time-delayed teleoperation," in *2015 IEEE/RSJ International Conference on Intelligent Robots and Systems*. Hamburg, Germany: IEEE, October 2015.
[14] B. Griffin and J. Grizzle, "Nonholonomic virtual constraints for dynamic walking," in *2015 54th IEEE Conference on Decision and Control*. Osaka, Japan: IEEE, December 2015.
[15] W. K. Chan, Y. Gu, and B. Yao, "Optimization of output functions with nonholonomic virtual constraints in underactauted bipedal walking control," in *2018 Annual American Control Conference*. Milwaukee, USA: IEEE, June 2018.
[16] J. C. Horn, A. Mohammadi, K. A. Hamed, and R. D. Gregg, "Nonholonomic virtual constraint design for variable-incline bipedal robotic walking," *IEEE Robotics and Automation Letters*, vol. 5, pp. 3691 – 3698, February 2020.
[17] R. D. Schafer, *An Introduction to Non-Associative Algebras*. New York: Dover Publications, 1996.
[18] L. D. Landau and E. M. Lifschitz, *Mechanics*, 3rd ed. Butterworth-Heinemann, January 1982.
[19] G. Golub and W. Kahan, "Calculating the singular values and pseudo-inverse of a matrix," *Journal of the Society for Industrial and Applied Mathematics: Series B, Numerical Analysis*, vol. 2, no. 2, pp. 204–224, 1965.
[20] M. Maggiore and L. Consolini, "Virtual holonomic constraints for euler-lagrange systems," *IEEE Transactions on Automatic Control*, vol. 58, no. 4, pp. 1001 – 1008, April 2013.
[21] S. Wirkus, R. Rand, and A. Ruina, "How to pump a swing," *The College Mathematics Journal*, vol. 29, no. 4, pp. 266 – 275, 1998.
[22] N. Metropolis, "The beginning of the monte carlo method," *Los Alamos Science*, pp. 125–130, 1987, 1987 special issue dedicated to Stanislaw Ulam.
[23] A. Mohammadi, M. Maggiore, and L. Consolini, "Dynamic virtual holonomic constraints for stabilization of closed orbits in underactuated mechanical systems," *Automatica*, vol. 94, pp. 112 – 124, August 2018.
[24] H. K. Khalil, *Nonlinear Systems*, 3rd ed. Upper Saddle River, NJ 07485: Prentice Hall, 2002.
[25] G. D. Birkhoff, *Dynamical Systems*. Colloquium Publications, 1927, vol. 9.